JPn Neuroscience
The Journal of Physiology
J Physiol 591.4 (2013) pp 899–918

Late-onset bursts evoked by mossy fibre bundle stimulation in unipolar brush cells: evidence for the involvement of H- and TRP-currents

F. Locatelli[1], L. Bottà[1], F. Prestori[1], S. Masetto[1] and E. D'Angelo[1,2]

[1] *Department of Neuroscience, Via Mondino 2, I-27100 Pavia, Italy*
[2] *Brain Connectivity Center (BCC), IRCCS C.Mondino, Via Mondino 2, I-27100 Pavia, Italy*

Key points

- Unipolar brush cells (UBCs) are specifically located in the vestibulo-cerebellum and are considered to play an important role in implementing a 'velocity storage' system. Nonetheless, their synaptic and excitable mechanisms are not fully understood.
- UBCs receive a giant synapse from a single mossy fibre generating a stereotyped excitatory postsynaptic potential (EPSP)-burst complex with early-onset (~2 ms) and high reliability. By using patch-clamp recordings in cerebellar slices of the rat vestibulo-cerebellum, we found that mossy fibre bundle stimulation also evoked (in ~80% of cases) a late-onset burst (after tens to hundreds of milliseconds) independent of EPSP generation.
- The late-onset burst delay decreased and its duration increased by raising stimulation intensity or the number of impulses. The late-onset burst was initiated by a slow depolarizing ramp driven by activation of an H-current (sensitive to ZD7288 and Cs^+) and of a TRP- (transient receptor potential) current (sensitive to SKF96365) and was occluded by intracellular cAMP.
- These results indicate that afferent activity can regulate H- and TRP-current gating in UBCs generating synaptically driven EPSP-independent responses, in which the delay rather than amplitude is graded with the intensity of the input pattern.
- Through the late-onset response, UBCs can translate the intensity of the input (coded as the number of active fibres and duration of their discharge) into output bursts with different delays. This time code could reverberate through the network along the chains made by UBCs with other UBCs and granule cells and may play an important role in regulating vestibulo-cerebellum functions.

Abstract Synaptic transmission at central synapses has usually short latency and graded amplitude, thereby regulating threshold crossing and the probability of action potential generation. In the granular layer of the vestibulo-cerebellum, unipolar brush cells (UBCs) receive a giant synapse generating a stereotyped excitatory postsynaptic potential (EPSP)-burst complex with early-onset (~2 ms) and high reliability. By using patch-clamp recordings in cerebellar slices of the rat vestibulo-cerebellum, we found that mossy fibre bundle stimulation also evoked (in ~80% of cases) a late-onset burst (after tens to hundreds of milliseconds) independent of EPSP generation. Different from the early-onset, the late-onset burst delay decreased and its duration increased by raising stimulation intensity or the number of impulses. Although depending on synaptic activity, the late-onset response was insensitive to perfusion of APV ((2*R*)-5-amino-phosphonopentanoate), NBQX (2,3-dioxo-6-nitro-tetrahydrobenzo(f)quinoxaline-7-sulfonamide) and MCPG ((*RS*)-α-methyl-4-carboxyphenylglycine) and did not therefore depend on conventional

DOI: 10.1113/jphysiol.2012.242180

glutamatergic transmission mechanisms. The late-onset response was initiated by a slow depolarizing ramp driven by activation of an H-current (sensitive to ZD7288 and Cs^+) and of a TRP- (transient receptor potential) current (sensitive to SKF96365), while the high voltage-activated and high voltage-activated Ca^{2+} currents (sensitive to nimodipine and mibefradil, respectively) played a negligible role. The late-onset burst was occluded by intracellular cAMP. These results indicate that afferent activity can regulate H- and TRP-current gating in UBCs generating synaptically driven EPSP-independent responses, in which the delay rather than amplitude is graded with the intensity of the input pattern. This modality of synaptic transmission may play an important role in regulating UBC activation and granular layer functions in the vestibulo-cerebellum.

(Resubmitted 1 August 2012; accepted after revision 5 November 2012; first published online 5 November 2012)
Corresponding author E. D'Angelo: Laboratory of Neurophysiology, Via Forlanini 6, 27100 Pavia, Italy. Email: dangelo@unipv.it

Abbreviations APV, (2*R*)-5-amino-phosphonopentanoate; HCN, hyperpolarization-activated Cyclic Nucleotide-gated channels; HVA, high voltage-activated; IR-DIC, infra-red differential interference contrast; LCA, loose cell-attached; LTS, low-threshold spike; LVA, low voltage-activated; MCPG, (*RS*)-α-methyl-4-carboxyphenylglycine; MFB, mossy fibre bundle; mGluRs, metabotropic glutamate receptors; NBQX, 2,3-dioxo-6-nitro-tetrahydrobenzo(f)quinoxaline-7-sulfonamide; TRP-channel, transient receptor potential channel; UBC, unipolar brush cell; Ih, H-current; CC, current clamp; VC, voltage clamp.

Introduction

Chemical synaptic transmission in the central nervous system is characterized by short synaptic delays, typically in the millisecond range, and by the graded nature of subthreshold responses regulating the probability of spike generation through spatio-temporal summation over multiple inputs (Shepherd, 2003). However, the connection between mossy fibres and unipolar brush cells (UBCs), which are concentrated in the vestibulo-cerebellum, represents a remarkable exception. UBCs emit a single short dendrite originating from the soma and terminating in a complex structure called 'brush', which receives a giant excitatory synapse from just one mossy fibre (Jaarsma *et al.* 1996; Mugnaini *et al.* 1997; Diño *et al.* 2000, 2001; Nunzi & Mugnaini, 2000; Nunzi *et al.* 2001; Kalinichenko & Okhotin, 2005). This synapse was reported to elicit an all-or-none response with little variability, early onset (about 2 ms) and protracted time course due to massive glutamate spillover (Rossi *et al.* 1995; Kinney *et al.* 1997).

A peculiar property of UBCs is the tight coupling between synaptic transmission and intrinsic excitable mechanisms. The initial depolarization produced by the excitatory postsynaptic potentials (EPSPs) was shown to activate a low-threshold spike (LTS) involving Ca^{2+} currents and sustaining action potential bursting (Diana *et al.* 2007). An open issue concerns the role of the H-current (I_h), which has also been reported in UBCs (Diana *et al.* 2007; Russo *et al.* 2007). The H-current is suited to drive slow depolarizations, contributing to low-frequency pacemaking and depolarizing rebounds in several neurons (e.g. Maccaferri & McBain, 1996; Neuhoff *et al.* 2002; Funahashi *et al.* 2003), including cerebellar Golgi cells (Forti *et al.* 2006; Solinas *et al.* 2007*a*,*b*) and Purkinje cells (Nolan *et al.* 2003, 2004), but its role in UBCs remains unclear. Another current that has been reported in UBCs is transient receptor potential (TRP) channel-mediated, and its activation was related to tonic membrane potential depolarization (Russo *et al.* 2007).

Here we show that mossy fibre bundle (MFB) stimulation, in addition to generating a typical early-onset response, in ∼80% of UBCs caused also (or uniquely) a late-onset burst, whose delay and duration depended on stimulus duration and intensity. The late-onset burst was initiated by a depolarizing ramp lasting tens to hundreds of milliseconds, which was driven by a cAMP-dependent H- and TRP-current activation. This result provides evidence for a mechanism of neurotransmission driven by voltage-dependent conductances and extends to central neurons the observation reported in peripheral ganglion neurons for the M current (Brown *et al.* 1981). Mossy fibre–UBC neurotransmission is thus peculiar in four ways: (i) there is a double early- and late-onset response, (ii) the early-onset response is all-or-none rather than graded, (iii) the late-onset response controls the delay and duration of burst generation rather than its probability of occurrence, and (iv) the late-onset response is based on regulation of intrinsic excitability rather than postsynaptic receptor gating. The late-onset UBC response could play an important role in storing temporal information in the vestibulo-cerebellar circuit.

Methods

Whole-cell and loose cell-attached patch-clamp recordings were performed from UBCs in the internal

granular layer of lobules I and X in acute rat cerebellar slices. The experimental procedures were approved by the ethical committee of the University of Pavia following the national guidelines of the MIUR (Ministero Italiano della Università e della Ricerca) and are consistent with the American Physiological Society's Guiding Principles in the Care and Use of Animals.

Experimental procedures

Cerebellar slices were obtained from 17- to 33-day-old Wistar rats (day of birth = 0). Rats were anaesthetized with halothane (Sigma, St Louis, MO, USA) and killed by decapitation. Parasaggital cerebellar slices (~220 μm thick) were cut from the cerebellar vermis using standard procedures (D'Angelo *et al.* 1993, 1995, 1998; Prestori *et al.* 2008) using a vibroslicer (Dosaka, Japan) in ice-cold potassium gluconate-based solution (in mM): 130 potassium gluconate, 15 KCl, 0.2 EGTA, 17 Hepes, 11 glucose; pH 7.4 with NaOH. The slices were then transferred to a carboxygenated Krebs solution and maintained at room temperature for at least 30 min before recordings. The Krebs solution had the following composition (in mM): 120 NaCl, 2 KCl, 1.2 $MgSO_4$, 26 $NaHCO_3$, 1.2 KH_2PO_4, 2 $CaCl_2$, 11 glucose, pH 7.4 with 95% O_2–5% CO_2. For all recordings, Krebs solution was added with the $GABA_A$ receptor antagonist 25 μM gabazine (SR95531) and the glycine receptor antagonist 1 μM strychnine (Duguè *et al.* 2005; Rousseau *et al.* 2012). In some experiments the following high-Mg^{2+}/low-Ca^{2+} extracellular solution was used to block synaptic transmission (in mM): 120 NaCl, 2 KCl, 4 $MgSO_4$, 26 $NaHCO_3$, 1.2 KH_2PO_4, 0.1 $CaCl_2$, 11 glucose, pH 7.4 with 95% O_2–5% CO_2. The slices were installed in the recording chamber mounted on the stage of an upright microscope (F2S; Zeiss Axioskop, Oberkochen, Germany) and viewed with a 63× water immersion objective. During recordings, the slices were maintained at room temperature and continuously superfused with carboxygenated Krebs solution, which proved convenient to improve the viability of the preparation. Control experiments aimed at verifying the presence of the late-onset response ($n = 15$) were performed at 37°C.

Electrical stimulation was performed by placing a bipolar tungsten electrode over the MFB in the granular layer (D'Angelo *et al.* 1993, 1995). The stimuli consisted of voltage pulses (0.25 ms, 5–15 V) organized in 100 Hz trains of varying intensity and length, as indicated. Patch-clamp recordings were obtained using an Axopatch 200-B amplifier and data were sampled through a DigiData 1200 and analysed with pClamp 9 software (Molecular Devices, Sunnyvale, CA, USA). The signals were low-pass filtered at 5 kHz and sampled at 20–40 kHz. Patch pipettes were pulled with a horizontal puller (Sutter Instruments, Novato, CA, USA) from thick-walled borosilicate glass capillaries (Hingelberg, Germany) and had a resistance of 7–10 MΩ when filled with the intracellular solution (in mM): 126 potassium gluconate, 4 NaCl, 15 glucose, 5 Hepes, 1 $MgSO_4.7H_2O$, 0.1 BAPTA, 3 ATP, 100 μm GTP; pH adjusted to 7.2 with KOH. The BAPTA-Ca buffer was prepared as explained previously (D'Angelo *et al.* 1995; Gall *et al.* 2003). In some experiments, 500 μM cAMP (Sigma) was added. To minimize pipette tip capacitance, pipettes were coated with Sylgard (Dow Chemical, Midland, MI, USA) and the bath level was kept as low as possible. Sealing was performed under visual control and cell identity was confirmed through the characteristic electroresponsiveness of the UBCs. In some experiments the patch pipette contained Alexa Fluor 488 (Invitrogen (Molecular Probes), Carlsbad, CA, USA) allowing us to take fluorescence images of the filled cells (excitation 480 nm, emission 535 nm, dichroic mirror 505 nm; Chroma Technology, Bellows Falls, VT, USA). The preparation was illuminated using a 50 W xenon lamp (Zeiss), acquired with a high-resolution camera (CoolSNAP HQ; Roper Scientific, USA) and analysed with MetaMorph software (Universal Imaging Corp., Downingtown, PA, USA).

After careful pipette capacitance cancellation (D'Angelo *et al.* 1995), the current transient elicited by a 10 mV hyperpolarizing step from a holding potential of −80 mV was analysed to monitor passive recording parameters. The transient decayed bi-exponentially, probably reflecting charging of two compartments corresponding to the UBC soma and brush. Bi-exponential fittings allowed us to estimate the electrode series resistance (R_s) the cell input capacitance (C_{in}) and the input resistance (R_{in}) using the equation:

$$I(t) = A_1 \times e(k - t/\tau_1) + A_2 \times e(k - t/\tau_2) + C \quad (1)$$

Series resistance (R_s) was calculated as $R_s = \tau_{VC}/C_{in}$, where $\tau_{VC} = \tau_1$ is the decay time constant of the current transient related to somatic charging. By using this method we estimated $R_s = 20.7 \pm 6.6$ MΩ, $C_{in} = 11.2 \pm 1.4$ pF and $R_{in} = 798.7 \pm 54.7$ MΩ ($n = 159$), consistent with previous reports in these same neurons (Diana *et al.* 2007; Russo *et al.* 2007). All current-clamp recordings were performed using the fast current-clamp mode of the amplifier to accelerate membrane charging (D'Angelo *et al.* 1995, 1998; Prestori *et al.* 2008). The resting membrane potential in non-discharging cells was measured over 50 ms in 12 consecutive traces. Intrinsic excitability was investigated by setting resting membrane potential at −80 mV and injecting 800 ms current steps (from −16 to 48 pA in 4–8 pA increments). In loose-seal recordings, the seal resistance was of the order of a few tens up to a few hundred megaohms. We verified that

this condition was suitable for revealing spontaneous action potentials by recording the spontaneous activity from Golgi cells (not shown), which normally show spontaneous firing (Forti *et al.* 2006).

SR95531 (25 μM), Cs^+ (2 mM), and mibefradil (10 μM) (Sigma), strychnine hydrochloride (1 μM), D-APV (D-(2*R*)-5-amino-phosphonopentanoate; 50 μM), NBQX (2,3-dioxo-6-nitro-tetrahydrobenzo(f)quinoxaline-7-sulfonamide; 2 μM) and ZD7288 (2–20 μM) (Tocris Cookson, Bristol, UK), SKF96365 (30 μM), MCPG ((*RS*)-α-methyl-4-carboxyphenylglycine; 500 μM) (Ascent Scientific, Avonmouth, UK) were prepared in water and stored at −20°C. Nimodipine (Sigma) was dissolved in DMSO at most 5 min before use, and the stock was used for a single experiment and applied in dark-room conditions. Drugs were bath-perfused after proper dilution in Krebs solution. As reported previously (Forti *et al.* 2006), ZD7288 action was allowed to stabilize for about 10 min and the effects were partially reversible after prolonged washout of the drug (>10 min, data not shown). Perfusion of nimodipine and mibefradil was protracted for 20 min before assessing their effects (Diana *et al.* 2007). In some experiments, we took care to apply mibefradil in the absence of SKF96365, which has been reported to block low voltage-activated (LVA) channels as well (Singh *et al.* 2010).

Data analysis and statistics

Analysis of current and voltage responses was performed off-line (Clampfit9; Molecular Devices). The spike threshold was measured by taking the first time derivative of voltage traces. The effectiveness of the slow-depolarizing ramp in triggering the late-response burst was evaluated by measuring four parameters: (i) the delay to first spike in the burst, (ii) the average slope of the ramp taken from beginning to spike threshold and (iii) the duration of the late-response burst. In addition, the effect of drugs was evaluated by comparing (iv) the value of the depolarization at the threshold of the first spike of the late-response burst before and after drug application. Of note, this parameter could be measured even when a drug blocked the spikes. All membrane potential values in the text and figures have been adjusted for liquid-junction potential (−10 mV inside the pipette).

The *I–V* curve for the ZD7288-sensitive component was fitted with the equation:

$$I(V) = [G_{Ih}\ (V_m - E_{Ih})]/[1 + \exp((V_m - V_{1/2})/k)], \quad (2)$$

where G_{Ih} is the maximum I_h conductance, V_m is the membrane potential, E_{Ih} is the Nernst potential for I_h, $V_{1/2}$ is the potential at which I_h conductance is half-activated and k is the voltage dependence of its activation (Hille & Schwarz, 1978; Rossi *et al.* 2006). Fittings with eqn (2) (e.g. Fig. 8*C*) were performed between −130 and −50 mV by least-squares minimization. The fitting procedure converged to the same result independent of initial parameters. The data obtained from eqn (2) were used to construct the normalized conductance curve, where $G(V) = I(V)/(V_m - E_{Ih})$:

$$G(V)/G_{Ih} = 1/[1 + \exp((V_m - V_{1/2})/k)] \quad (3)$$

Data sets were usually compared using Student's *t* test. Values of $P < 0.05$ were considered significant. The data in Fig. 9 were first assessed for normality with the Lilliefor's test, then statistical significance in the comparisons of data groups was tested with the non-parametric Kruskal–Wallis ANOVA test. In the text, data are reported as mean ± SEM, and *n* indicates the number of observations.

Results

UBC intrinsic electroresponsiveness

Patch-clamp recordings were obtained from 159 UBCs, 154 located in lobus X (nodulus) and five in lobus I (lingula), in cerebellar slices of 17- to 33-day-old rats. UBCs, which have a soma larger than granule cells but smaller than Golgi cells, were visually identified using infrared differential interference contrast (IR-DIC) video-microscopy. In selected cases ($n = 8$), UBCs were filled with Alexa Fluor 488 making their characteristic brush visible in fluorescence images and confirming the IR-DIC identification (Fig. 1*A*). Further distinctive properties derived from the electrophysiological analysis of current transients elicited by 10 mV hyperpolarizing voltage steps (see Methods) and of intrinsic electroresponsiveness are shown in Fig. 1*B*.

In the present recordings, 92% of the UBCs were silent at rest, with a membrane potential of −67.5 ± 4.7 mV ($n = 147$) and spiking threshold at −55.8 ± 4.8 mV ($n = 147$). The UBCs showing repetitive firing at rest (average frequency 11.7 ± 8.3 Hz, $n = 12$) (Russo *et al.* 2007) were not further considered in the continuation of this work. Of the remaining 139 UBCs, 133 responded to MFB stimulation and were used either for current-clamp (CC) ($n = 115$) or voltage-clamp (VC) recordings ($n = 18$).

Depolarizing current steps from holding membrane potentials of −80.2 ± 1.2 mV ($n = 5$) caused an LTS surmounted by a burst of action potentials (Fig. 1*B*). The LTS could be followed by a sustained discharge when depolarization was intense. Depolarization from holding potentials of −55.7 ± 1.2 mV ($n = 5$) caused a marked weakening of LTS and of the spike burst. At the same time, the burst spike frequency changed from 46.5 ± 5.7 to 12.3 ± 2.4 Hz (e.g. Fig. 1*C*). In these experiments,

the excitable response was generated using the minimal current leading to spike threshold. The observation that UBCs, rather than generating an LTS surmounted by a robust burst, generated a weak spike discharge instead was consistent with inactivation of a low-threshold calcium current. Stronger depolarizations (above −40 mV) caused tonic firing (data not shown). The above results are consistent with UBCs expressing LVA Ca^{2+} currents contributing to LTS generation, the latter being inactivated by cell depolarization (Diana *et al.* 2007). Hyperpolarizing current steps produced slow sagging inward rectification (Fig. 1*B*, see inset), consistent with observations showing that UBCs express the H-current (Diana *et al.* 2007; Russo *et al.* 2007).

Note that, in similar recordings conditions, GrCs are silent at rest, while GoCs show low-frequency pacemaking (in the 4 Hz range). Moreover, LTS are not observed in GrCs (D'Angelo *et al.* 1995, 1997, 1998) or GoCs (Dieudonne, 1998; Forti *et al.* 2006) at this same developmental stage, setting a clear difference between UBCs and these neuronal types.

UBC synaptic activation: early-onset and late-onset responses

A single giant synapse connects mossy fibre terminals with the UBC brush (Rossi *et al.* 1995; Mugnaini *et al.* 1997; Nunzi & Mugnaini, 2000; Nunzi *et al.* 2001) and the response to MFB stimulation is all-or-none in nature (Rossi *et al.* 1995). Indeed, when UBCs were recorded from a membrane potential of −80 mV, a single stimulus pulse to the MFB elicited with short delay an EPSP (1.71 ± 0.32 ms, $n = 22$) triggering an LTS surmounted by an action potential burst (Fig. 2*A*, top; see also inset). This early-onset response was clearly related to the underlying excitatory postsynaptic current (EPSC) (Fig. 2*A*, bottom), which showed kinetics similar to those reported previously (Rossi *et al.* 1995; Diana *et al.* 2007), and probably consists of a first rapid transient AMPA-receptors current followed by the slower NMDA-receptors current. Clearly, the EPSC primes and sustains the EPSP-burst complex, which then assumes a stereotyped configuration due to the intervention of voltage-dependent currents.

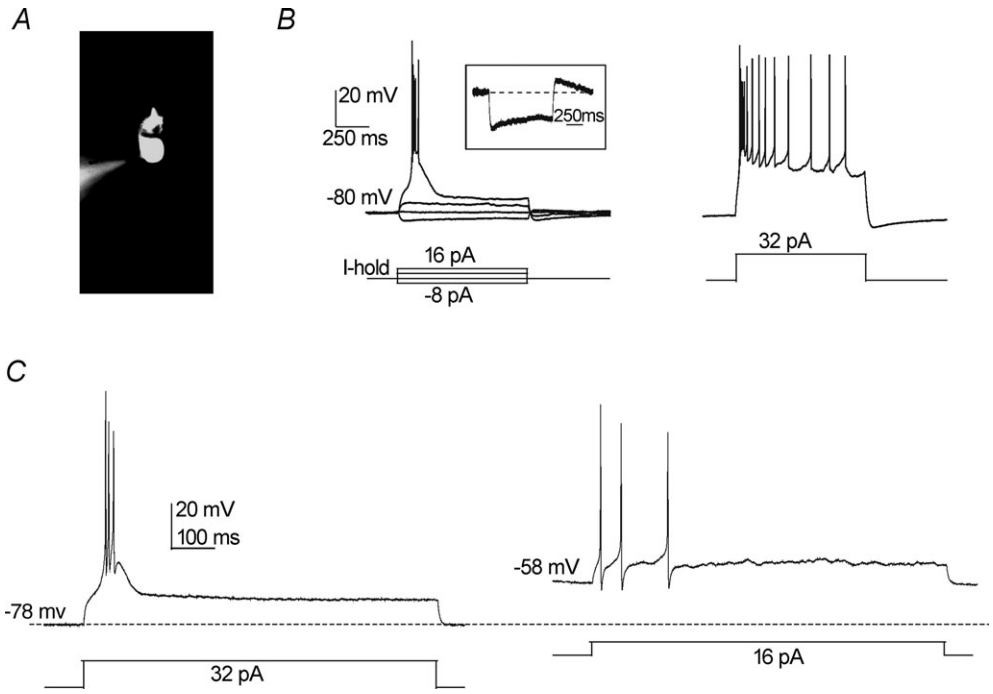

Figure 1. UBC electroresponsiveness
A, photomicrograph of a UBC filled with Alexa Fluor 488 in whole-cell configuration (the pipette tip is evident on the left). A short dendrite departs from the soma and terminates with the 'brush', an enlarged and irregular structure composed of numerous dendrioles. *B*, CC response recorded from the same UBC shown in *A*. The UBC membrane potential was maintained at −80 mV by constant current injection (I-hold), and currents steps were applied according to the protocol shown. Depolarizing current steps of sufficient intensity produced a low-threshold spike (LTS) surmounted by a brief burst of action potentials (left panel), which was followed by a slowly adapting action potential discharge when the intensity of the stimulus was increased further (right panel). In the hyperpolarizing direction, the UBC response showed a clear sag, indicative of H-current activation. This is also consistent with the rebound depolarization seen upon return to −80 mV (the inset shows the response to the −8 pA current step in isolation). *C*, CC response recorded from a UBC maintained at −78 mV (left) or −58 mV (right). Note the absence of LTS in the latter case.

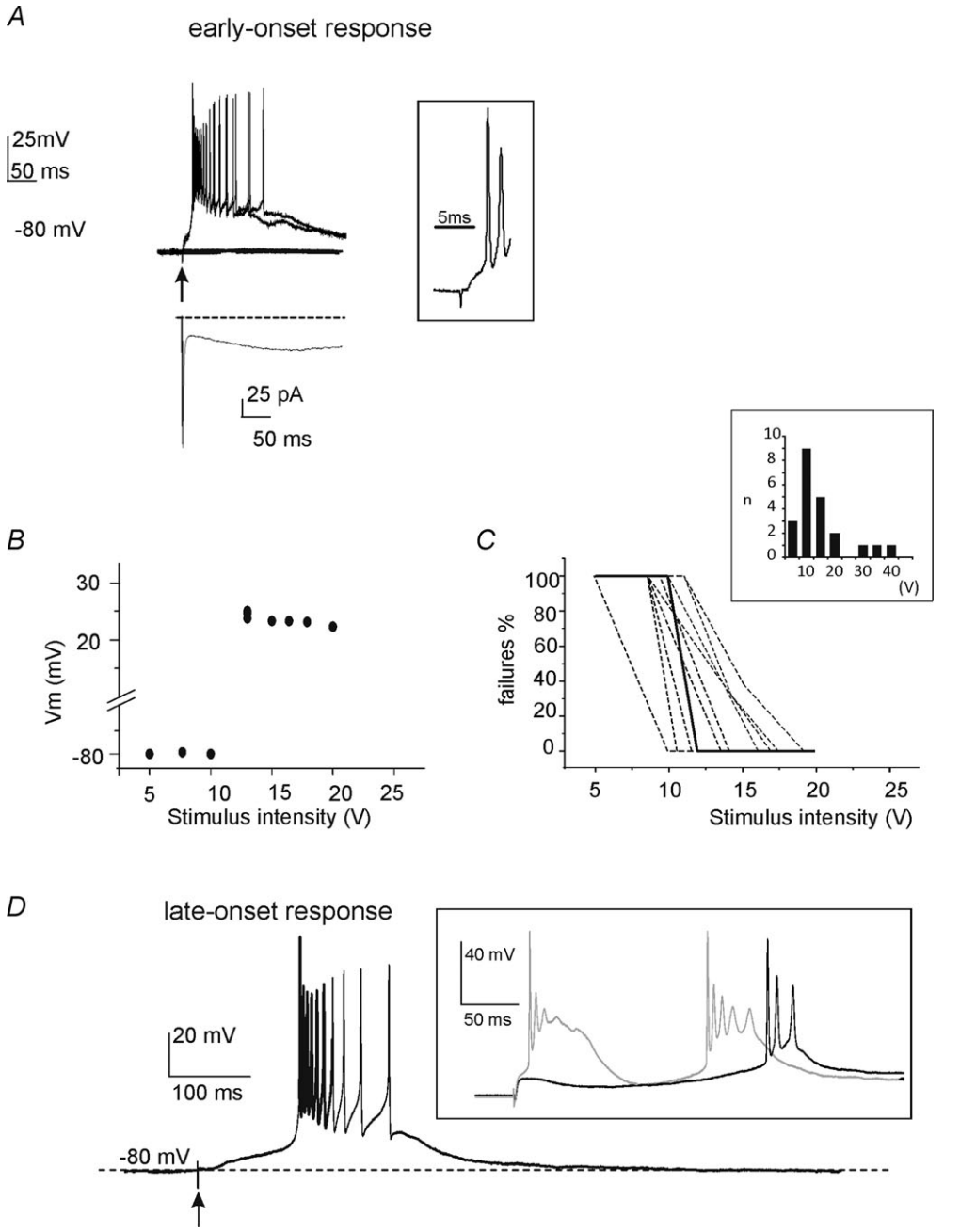

Figure 2. Early- and late-onset response elicited by single-pulse MFB stimulation
A, typical voltage responses elicited by single pulse stimuli to the MFB of different intensity (5–20 V). Arrow indicates the time of pulse delivery. Following pulses of enough intensity, the UBC generated an action potential burst with a short latency (<2 ms, see inset at right), consistent with classic monosynaptic delay. The bottom trace shows the VC response recorded from the same UBC following analogous MFB stimulation. The elicited EPSC presented a fast transient inward current component followed by a much slower one, consistent with AMPA and NMDA receptor activation, respectively (see text). *B*, scatter plot showing the amplitude of UBC depolarization as a function of MFB stimulus intensity (same cell as in *A*). Note that the early-onset response occurred suddenly over a sharp threshold and that, once elicited, its amplitude did not increase further with increasing stimulus intensity, indicating that the early-onset response was all-or-none. *C*, percentage of early-onset response failures as a function of pulse stimulus intensity in six different UBCs. The dashed line refers to the cell shown in *A* and *B*. Note the sharp transition from failures to full-blown responses. The bar graph (inset) shows the intensity of mossy fibre bundle stimulation at which the early-onset response was elicited in the 22 recordings covered in this section. *D*, typical late-onset response recorded from a different UBC. MFB stimulation elicited a slow depolarizing ramp finally triggering a spike burst with a considerably long delay (>100 ms; arrow indicates the time of MFB stimulus). The inset shows the early- and late-onset responses recorded from another UBC, indicating they can coexist in the same cell.

This early-onset response switched suddenly from failure to a full EPSP-burst complex by raising the stimulus intensity (Fig. 2*B* and *C*; the range of intensities eliciting the early onset response in the 22 cells covered in this section is illustrated in Fig. 2*C*, inset). Interestingly, in some UBCs ($n = 9$), the stimulus did not elicit any EPSPs but was followed by a slow depolarizing ramp leading to a late-onset response with delay that could be as long as ~50–500 ms (Fig. 2*D*). Yet in other UBCs ($n = 3$), the early-onset response was followed by a slow depolarizing ramp leading to the late-onset response (Fig. 2*D*, inset). A similar behaviour was observed in response to stimulus trains, as documented below.

Given its peculiar nature, we ascertained that the late-onset response was due to synaptic transmission through effective axonal excitation and neurotransmitter release. To this end, the early-onset and late-onset responses were elicited by 10 pulse trains and the ordinary extracellular solution was then substituted with one with a high Mg^{2+}/Ca^{2+} ratio (4 mM Mg^{2+}/0.1 mM Ca^{2+}, see Methods; $n = 7$). This solution blocked both the early- and the late-onset response almost simultaneously and in a reversible manner (Fig. 3). Thus, since blockage of the early-onset response probably depended on failure of neurotransmitter release at the mossy fibre terminals, the simultaneous blockage of the late-onset response also had to reflect failure of a synaptic calcium-dependent mechanism as well. It should be noted that, using an almost identical stimulation protocol, mossy fibre excitability was not compromised by high Mg^{2+}/Ca^{2+} ratios (Silver *et al.* 1996; Maffei *et al.* 2002; Sola *et al.* 2004; Mapelli *et al.* 2009). Simultaneous blockage of the early-onset and late-onset response was also obtained after application of 1 μM tetrodotoxin at the end of recordings ($n = 5$, data not shown), further demonstrating the absence of direct influence of the stimulus on UBC excitation.

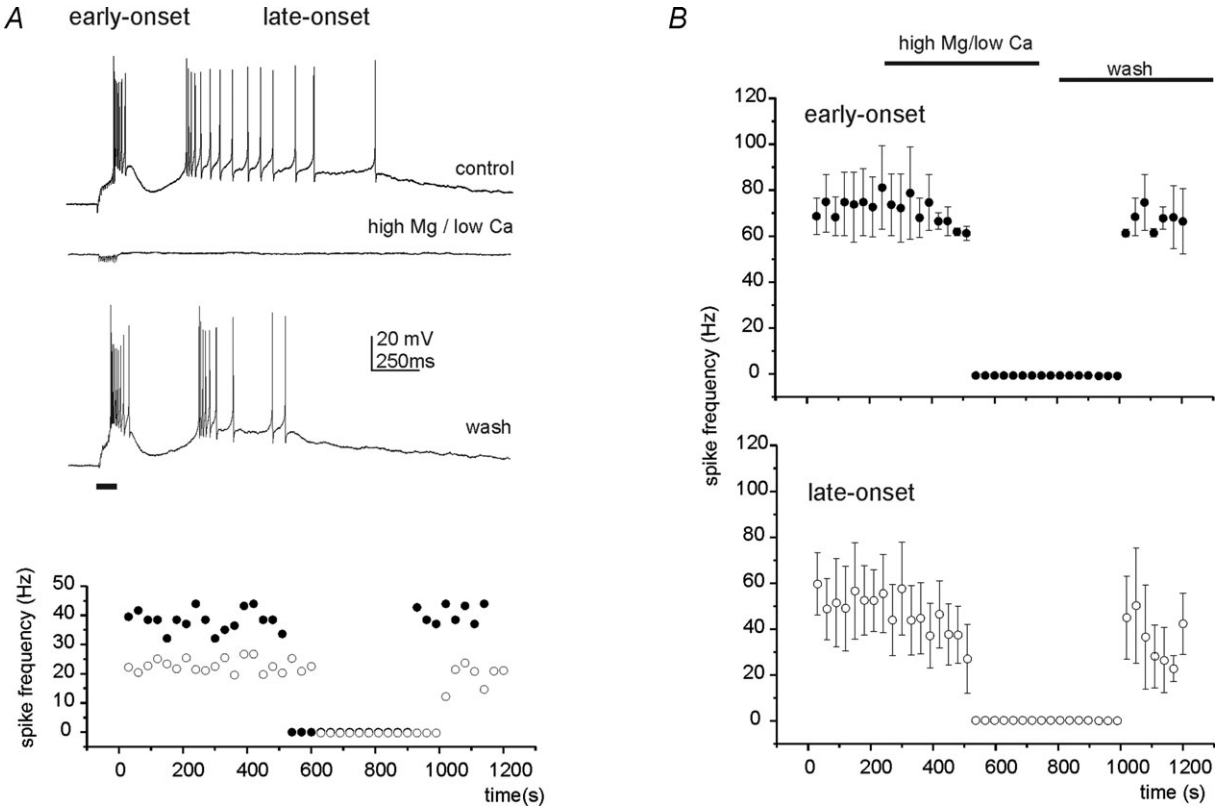

Figure 3. The early- and late-onset responses are suppressed by perfusing a high-Mg $^{2+}$/low-Ca^{2+} extracellular solution
A, the top trace shows the voltage response elicited in a UBC by a train stimulus delivered to the MFB. Here and in the next experiments, train frequency was 100 Hz. After changing the extracellular solutions in the bath (control) with the high-Mg^{2+}/low-Ca^{2+} extracellular solution (see Methods), both the early- and the late-onset responses disappeared (middle trace). The effect was reversible after wash (bottom trace). The horizontal bar at the bottom, here and in the next figures, indicates the train stimulus length. The scatter plot at the bottom illustrates the spike frequency in the early-onset (filled symbols) and in the late-onset (open symbols) response during the course of the same experiment. *B*, scatter plot summarizing the average spike frequency in the early-onset ($n = 3$) and late-onset ($n = 4$) response following perfusion of the high-Mg^{2+}/low-Ca^{2+} extracellular solution. Note that the high-Mg^{2+}/low-Ca^{2+} extracellular solution almost completely suppressed the synaptic response.

Since UBC response properties might have been influenced by the whole-cell configuration, control recordings were performed in loose cell-attached (LCA) configuration Forti *et al.* 2006). None of the UBCs recorded in LCA ($n = 7$) configuration fired spontaneously, although action potentials could be generated by MFB stimulation (Fig. 4). The different combinations of early- and late-onset responses found in whole cells were also found in LCA ($n = 7$) mode. The first spike delay of the late-onset response in these recordings was 697.02 ± 228.84 ms ($n = 4$) and its duration was 5580 ± 2300 ms ($n = 4$). Thus, the late-onset response could be evoked from resting UBCs in the absence of potential changes imposed by intracellular dialysis.

Regulation of the late-onset response by stimulus trains

The effect of train stimulation was carefully analysed in a group of UBCs maintained at the holding potential of −80 mV (Fig. 4). From this potential, a single pulse elicited just a sub-threshold depolarization (mean EPSP amplitude $= 2.8 \pm 1.8$ mV; $n = 93$), so that the effect of EPSP temporal summation could be demonstrated. In these cells, a train of stimuli could evoke either the early-onset and the late-onset response together ($n = 27$) or the late-onset response alone ($n = 69$) (Fig. 5*A* and *B*). Thus, the late-onset response depended on synaptic transmission but not on the presence of the early-onset response and of the associated membrane potential changes.

While the early-onset response yields an all-or-none EPSP–spike complex in UBCs, the behaviour of the late-onset response in this respect was unknown and needed to be clarified. By increasing intensity of the stimulus train, the delay of the late-onset response decreased, while its duration increased (Fig. 5*A*). An analogous effect on the late-onset response was also observed when the number of pulses was increased (Fig. 5*B*). Likewise, the delay of the late-onset response elicited by a stimulus train was always shorter than that elicited by a single pulse (Fig. 5*C*, left). Finally, the delay could be reduced so much that the early- merged with the late-onset response, when the two were present together (Fig. 5*C*, right). Thus, in contrast to the all-or-none nature of the early-onset response, the late-onset response showed a graded regulation of ramp and burst properties depending on stimulus intensity and on the number of spikes in the stimulus train.

The dependence of the late-onset response from stimulus intensity is quantified in Fig. 5*D*. On average, while raising stimulus intensity, the ramp slope increased by $92.6 \pm 50.2\%$ ($P < 0.0005$, $n = 12$), the delay decreased by $48.7 \pm 3.8\%$ ($P < 0.001$, $n = 12$), burst duration increased by $31.5 \pm 18.3\%$ ($P < 0.05$, $n = 12$) and burst frequency increased by $18.3 \pm 4.2\%$ ($P < 0.005$, $n = 12$) (paired *t* test between smallest and largest intensity in each cell; Fig. 5*E*). While slope and burst delay (which were inversely correlated) indicate the intensity of the ramp-generating mechanism, burst duration and frequency indicate the intensity of the burst-generating mechanism. In the following we preferentially use ramp slope and burst duration as representative parameters of the late-onset response processes.

The late-onset response does not depend on ionotropic or metabotropic glutamate receptors

The UBC postsynaptic responses were shown to involve NMDA and AMPA glutamate receptors (Rossi *et al.* 1995; Nunzi *et al.* 2001). Consistent with the kinetics

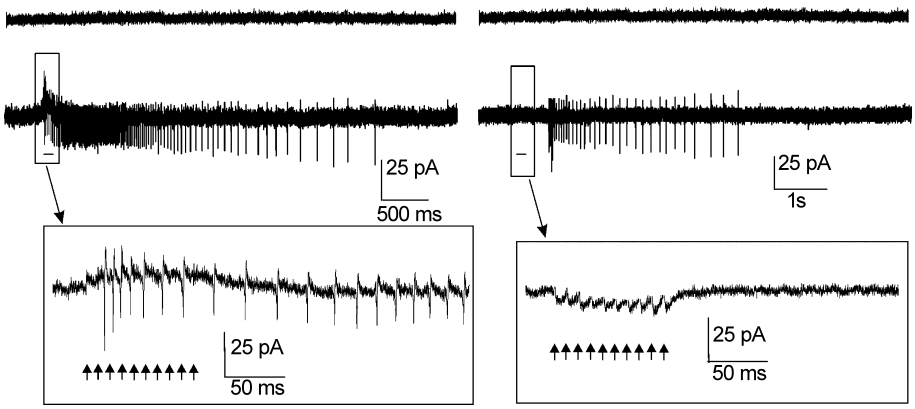

Figure 4. Early- and late-onset response recorded in loose cell-attached (LCA) configuration
The left panel shows a representative LCA recording from a UBC showing the early-onset response only. When a train of 10 pulses (arrows) was delivered to the MFB, a long-lasting discharge of action currents was recorded beginning during the train (see inset; arrows indicate train pulses). The right panel shows the late-onset response recorded from a different UBC. Note that no action currents were elicited during and shortly after the train. No spike activity was observed in either cell in the absence of MFB stimulation.

of EPSCs recorded in some UBCs (Fig. 2*A*), when APV (50 μM) and NBQX (2 μM) were co-perfused on UBCs showing both the early-onset and the late-onset response (Fig. 6*A*), these receptor antagonists blocked the early-onset response (the LTS-burst complex disappeared leaving residual depolarization of < 10 mV at the end of the train) but left the late-onset response unaffected ($n = 7$). In the UBCs showing only the late-onset response, NBQX and APV were similarly ineffective ($n = 4$; data not shown). The ramp slope was 0.032 ± 0.007 mV ms^{-1} before and 0.032 ± 0.062 mV ms^{-1} after APV and NBQX ($P = 0.7$, $n = 4$) and burst duration was 1171.3 ± 792.8 ms before and 743.4 ± 642.9 ms after APV and NBQX perfusion ($P = 0.5$, $n = 4$). Therefore, the late-onset response was not sustained by ionotropic glutamate receptors.

UBCs also express metabotropic glutamate receptors (mGluRs) of group I and II (Rousseau *et al.* 2012), and class II mGluRs have been shown to couple to inward rectifier K^+ currents hyperpolarizing the cell (Russo *et al.*

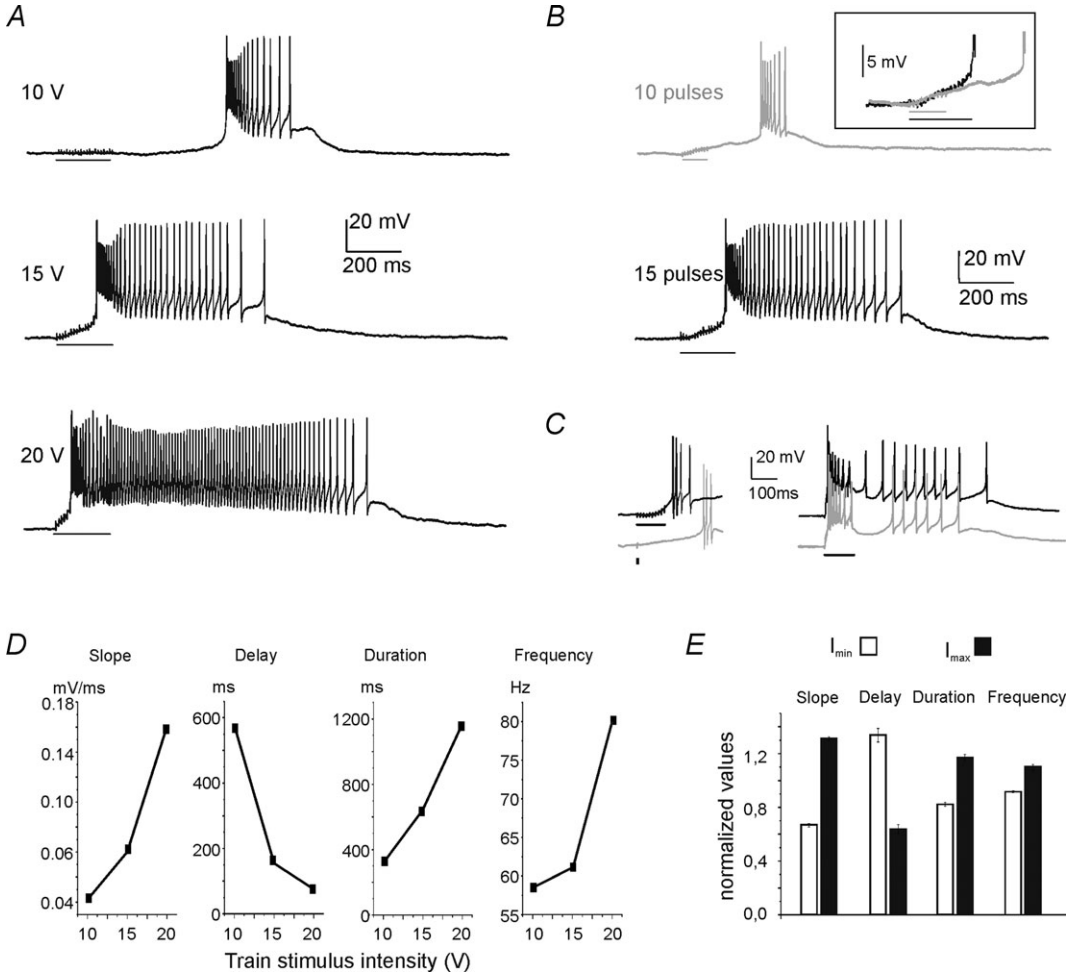

Figure 5. The late-onset response is graded with MFB stimulation
A, late-onset responses evoked in a UBC by trains of 20 pulses delivered to the MFB. Note that by increasing the stimulus intensity, the delay of the response decreased while its duration increased. *B*, late-onset responses evoked in a UBC by trains of different length. Note that by increasing the number of pulses, the delay of the response decreased while its duration increased. The different time course of the depolarizing ramp can be appreciated by overlapping the first part of the tracings (inset). *C*, left panel: the late-onset responses evoked by a single pulse of 15 V (grey trace) had a longer delay and shorter duration compared to that evoked by a train of pulses of the same intensity (black trace). Right panel: the late-onset response approached the early-onset response as the stimulus intensity was increased from 10 to 20 V (grey trace). *D*, graphs illustrating the relationship between the intensity of the train stimulus to the MFB and ramp slope, burst delay, burst duration and burst spike frequency of the late-onset response (same UBC as in *A*). *E*, histogram showing normalized values for ramp slope, burst delay, burst duration and burst spike frequency measured for the voltage responses elicited by positive current steps of just-above-threshold intensity (I_{min}) and of maximal intensity (I_{max}) in 12 UBCs showing the late-onset response alone. Current steps were delivered from a holding voltage of -80 mV. The data Y have been normalized using the equations $Y_{min}/((Y_{min}+Y_{max})/2)$ and $Y_{max}/((Y_{min}+Y_{max})/2)$.

2008). In other neurons, such as Purkinje cells, group I mGluRs have been shown to couple to intracellular transduction systems controlling slow depolarization through TRP-channels (Batchelor *et al.* 1994; Tempia *et al.* 2001; Kim *et al.* 2003; Hartmann & Konnerth, 2008). However, when the mGluR blocker MCPG (which is more potent on group I mGluRs) (500 μM) was perfused in the bath, neither ramp slope (0.061 ± 0.028 mV ms^{-1} before and 0.064 ± 0.031 after MCPG; $n = 5$, $P = 0.8$) nor burst duration (1196.5 ± 469.4 ms before and 1056.4 ± 505.1 ms after MCPG; $n = 5$, $P = 0.6$) showed any significant change (Fig. 6*B*). In four other UBCs tested, the antagonist LY341495 (which is more potent on group II mGluRs) was similarly ineffective (data not shown). Therefore, mGluRs do not appear to regulate the UBC late-response burst substantially.

H- and TRP-current control of the late-onset response

A distinguishing feature of the late-onset response is the slow depolarizing ramp, starting soon after MFB stimulation and increasing in steepness until activating the spike burst. The ramp could result either from activation of a depolarizing current or from inhibition of a hyperpolarizing current active in the subthreshold region. A first indication on the nature of the ionic processes generating the ramp was obtained by measuring the amplitude of voltage deflections induced by small hyperpolarizing current pulses. Along the depolarizing ramp (from 10 ms after the stimulus to 10 ms before the LTS) the voltage response elicited by these steps decreased by 44.9% (from 2.21 ± 0.63 to 1.24 ± 0.41 mV, $n = 8$, $P < 0.001$, paired *t* test). This indicated that the ramp was sustained by a decrease in input resistance supporting the opening of depolarizing channels (Fig. 7*A*).

A second indication of the mechanism involved in sustaining the ramp was provided by comparing the response generated by MFB stimulation while keeping the same UBC either at -79.4 ± 1.8 mV ($n = 4$) or at -51.9 ± 0.9 mV ($n = 4$) (Fig. 7*B*). The UBC burst frequency was reduced from 54.7 ± 6.0 to 9.4 ± 0.4 Hz ($P < 0.01$; $n = 4$, paired *t* test), without significant change in the slope of the depolarizing ramp, which measured 0.08 ± 0.05 and 0.07 ± 0.03 mV ms^{-1} ($P = 0.8$; $n = 4$, paired *t* test). This result indicates that the slope of the depolarizing ramp did not depend on voltage-inactivated currents such as the LVA calcium current, which could, however, control burst frequency (cf. Fig. 1).

A candidate current sustaining the depolarizing ramp is the H-current, which is active in the voltage range below –50 mV and is expressed in UBCs (Diana *et al.* 2007; Russo *et al.* 2007). Therefore, we tested the effect of ZD7288 on the late-onset response (Fig. 8*A* and *B*). ZD7288 is a bradicardic agent and a potent and selective H-current blocker (reported IC_{50} for H-current block in brain slices is: 10.5 μM (Gasparini & DiFrancesco, 1997) and 2.3 μM (Dickson *et al.* 2000; Neuhoff *et al.* 2002)). Consistent with H-current being active in the subthreshold region, 2–20 μM ZD7288 hyperpolarized the UBCs by 4.13 ± 0.72 mV from the holding potential of -80 mV ($n = 9$; $P < 0.0005$, paired *t* test). Moreover, the slope of the depolarizing ramp leading to the spike burst decreased from 0.08 ± 0.01 to 0.03 ± 0.02 mV ms^{-1} ($n = 9$; $P < 0.01$, paired *t* test) (e.g. Fig. 8*B*). The decrease in ramp slope was still obvious when UBCs were repolarized to the pre-ZD7288 level by current injection (not shown). This indicates that

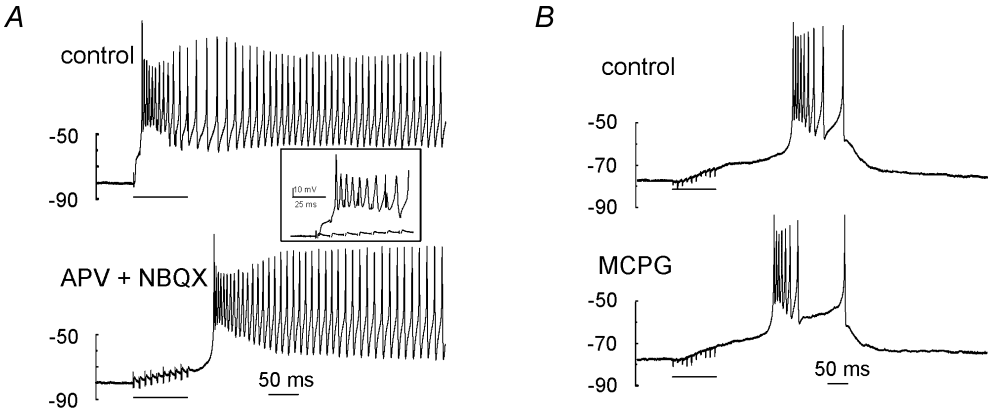

Figure 6. Effects of glutamate receptor blockers on the early- and late-onset response
A, post-synaptic responses evoked by a train of 10 pulses to the MFB in a UBC showing both the early- and the late-onset response, in control condition (top trace) and after perfusion of APV plus NBQX in the bath (bottom trace). Note that the early-onset response was blocked by the NMDA/AMPA receptor antagonists, thus unmasking the late-onset response. The inset shows the stimulus region in greater detail, demonstrating abolition of EPSPs following drug perfusion. *B*, post-synaptic responses evoked by a train of 10 pulses to the MFB in a UBC showing only the late-onset response, in control condition (top trace) and after perfusion of MCPG in the bath (bottom trace). Note the lack of effect of MCPG.

the H-current can regulate the delay of the late-onset burst by controlling the slope of the depolarizing ramp. Accordingly, in these same cells, ZD7288 strongly reduced the sag during hyperpolarization (measured as the difference between the maximum voltage deflection and the voltage attained at the end of the current step: from 2.61 ± 0.72 to 0.65 ± 0.74 mV, $n = 5$; $99.4 \pm 0.7\%$ reduction, $P < 10^{-5}$, paired t test) and the subsequent rebound depolarization (from 3.01 ± 1.12 to 0 mV, $n = 5$; 100% reduction, $P < 10^{-5}$) (Fig. 8*B*). Moreover, the slope of the depolarizing ramp leading to the spike burst decreased from 0.05 ± 0.01 to 0.02 ± 0.01 mV ms^{-1} ($n = 4$; $P < 0.05$, paired t test). The inorganic H-current blocker Cs^+ (2 mM; $n = 4$; Fig. 8*A*) had a similar effect as that of ZD7288 as far as the depolarizing ramp parameters were considered (see Table 1). However, Cs^+ blocked burst firing more effectively than ZD7288, showing the slow depolarization underlying the late-response burst, suggesting Cs^+ had additional effects on UBC channels involved in burst generation. These observations also tended to rule out spurious effects of ZD7288 on K^+ and Ca^{2+} currents. The potential ZD7288 block of K^+ currents (e.g. in subthalamic nucleus neurons; Do & Bean, 2003) would produce a depolarization rather than a hyperpolarization of cell resting membrane potential. A ZD7288 block of LVA Ca^{2+} currents (e.g. in pyramidal neurons; (Sanchez-Alonso *et al.* 2008) has been reported, although at much higher concentration (20% block at 20 μM ZD7288) and was therefore unlikely to play any relevant role here, also because LVA current inactivation or block did not significantly affect the depolarizing ramp (see Figs 7*B* and 8*B*).

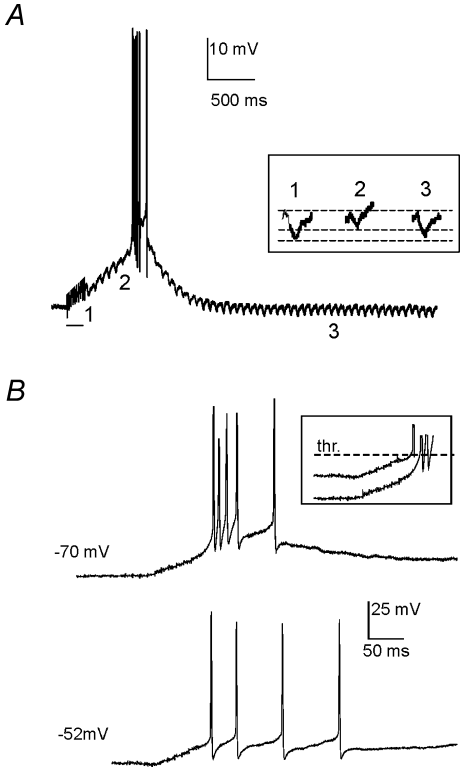

Figure 7. Cell membrane processes involved in late-onset response generation
A, to monitor UBC input resistance during the late-onset response, negative square pulses (8 pA, 50 ms) were delivered at 50 ms intervals after MFB stimulation (10 pulses of 20 V). Note that the hyperpolarizing transients generated by the negative steps decreased during the depolarizing ramp and returned to their initial amplitude after the burst. The voltage deflections elicited by three hyperpolarizing steps at different times during the late-onset response are shown in greater detail in the inset (1, control condition; 2, depolarizing ramp; 3, repolarization). *B*, late-onset responses elicited in the same UBC by train stimuli to the MFB (10 pulses of 15 V) at two different holding membrane potentials. Note that when the holding voltage was −80 mV the depolarizing ramp preceded a full-blown burst, while from −52 mV the burst was markedly weakened. However, the slope of the depolarizing ramp was almost the same (see inset).

Although these results demonstrate the inhibitory action of H-current blockers, other currents could also take part in generating the depolarizing ramp leading to the late-onset burst. One potential candidate is the TRP-current, which was shown to generate slow responses in Purkinje cells (Batchelor *et al.* 1994; Kim *et al.* 2003; Hartmann & Konnerth, 2008) and is expressed in UBCs (Russo *et al.* 2007). Indeed, application of the TRP-channel blocker SKF96365 (30 μM) inhibited the generation of the late-onset burst (Fig. 8*A*), which disappeared in most cases ($n = 4$ over five UBCs). The slope of the depolarizing ramp leading to the spike burst decreased from 0.03 ± 0.01 to 0.01 ± 0.003 mV ms^{-1} ($n = 5$; $P < 0.01$, paired t test). However, SKF96365 did not modify the sag (from 1.35 ± 0.31 to 1.31 ± 0.55 mV, $n = 5$; $P = 0.49$, paired t test) and rebound (from 1.28 ± 0.22 to 1.26 ± 0.24 mV, $n = 5$; $P = 0.47$, paired t test) generated by the H-current in hyperpolarizing responses (Fig. 8*B*). In the same UBCs, the holding current did not change significantly ($-24.54 \pm 11.67\%$, $n = 4$, $P = 0.17$), suggesting that TRP-channels mostly opened after MFB stimulation rather than contributed to background UBC conductance. The combined application of ZD7288 (2 μM) and SKF96365 (30 μM) ($n = 5$; Fig. 8*B*) almost completely abolished not just the late-onset burst but also the underlying slow depolarization, generating an effect significantly larger than that of the individual blockers alone (see Table 1).

Ca^{2+} currents were shown to play a role in UBC burst generation following somatic current injection (Diana *et al.* 2007). Application of the high voltage-activated (HVA) current blocker nimodipine (20 μM, $n = 4$) slightly (but not significantly) reduced spike frequency in the burst associated with the late-onset response (Fig. 8*C*), while a more evident spike-frequency reduction was caused by subsequent application of the LVA current blocker mibefradil (10 μM; Fig. 8*C*; $n = 4$). In the burst, spike frequency changed from 49.5 ± 15.6 to 15.5 ± 5.9 Hz

($P < 0.001$; $n = 4$, paired t test) after mibefradil, consistent with a contribution of LVA channels to the burst. However, neither nimodipine nor nimodipine and mibefradil perfused together changed the late-onset burst latency or the steepness of the depolarizing ramp, which measured 0.13 ± 0.05 and 0.10 ± 0.03 mV ms^{-1} ($P = 0.5$; $n = 4$, paired t test) (see Table 1). Thus, Ca^{2+} currents could regulate spike discharge within the late-onset-burst but did not regulate the depolarizing ramp.

Homogeneity of the late-onset response in pharmacological experiments

The distribution of two parameters defining the ramp (ramp slope) and the burst (burst duration) was analysed in all 93 UBCs showing the late-onset response to a 20 pulse-train stimulus to the MFB. All the data used in the plot in Fig. 9 were obtained from UBCs recorded in the same control conditions before being further used for pharmacological experiments. Plotting ramp slope *vs.* burst duration ($n = 93$, $R^2 = 0.001$, $P(F) = 0.32$) did not show significant correlation between the two, suggesting that the ramp and the burst were controlled by independent mechanisms (Fig. 9). The average ramp slope measured 0.05 ± 0.01 mV ms^{-1} ($n = 93$) and the average burst duration measured 987.2 ± 96.1 ms ($n = 93$).

On visual inspection, distribution of the data did not reveal any obvious clustering in the cell sub-groups used for pharmacological experiments. The data were not normally distributed (Lilliefor's test, NS). In the Kruskal–Wallis non-parametric ANOVA test, ramp slope and burst duration values were not significantly different from the general population for any of the sub-groups (APV+NBQX, MCPG, LY341495, ZD7288, Cs^+, nimodipine+mibefradil, SKF96365, SKF96365+ZD7288; $P > 0.05$ for all data sets). Therefore, there was no evidence for subclasses of UBCs with respect to the late-onset response.

H- and TRP-current changes following mossy fibre bundle stimulation

The pharmacological observations reported in Fig. 8 suggested that the H- and TRP-current increased following

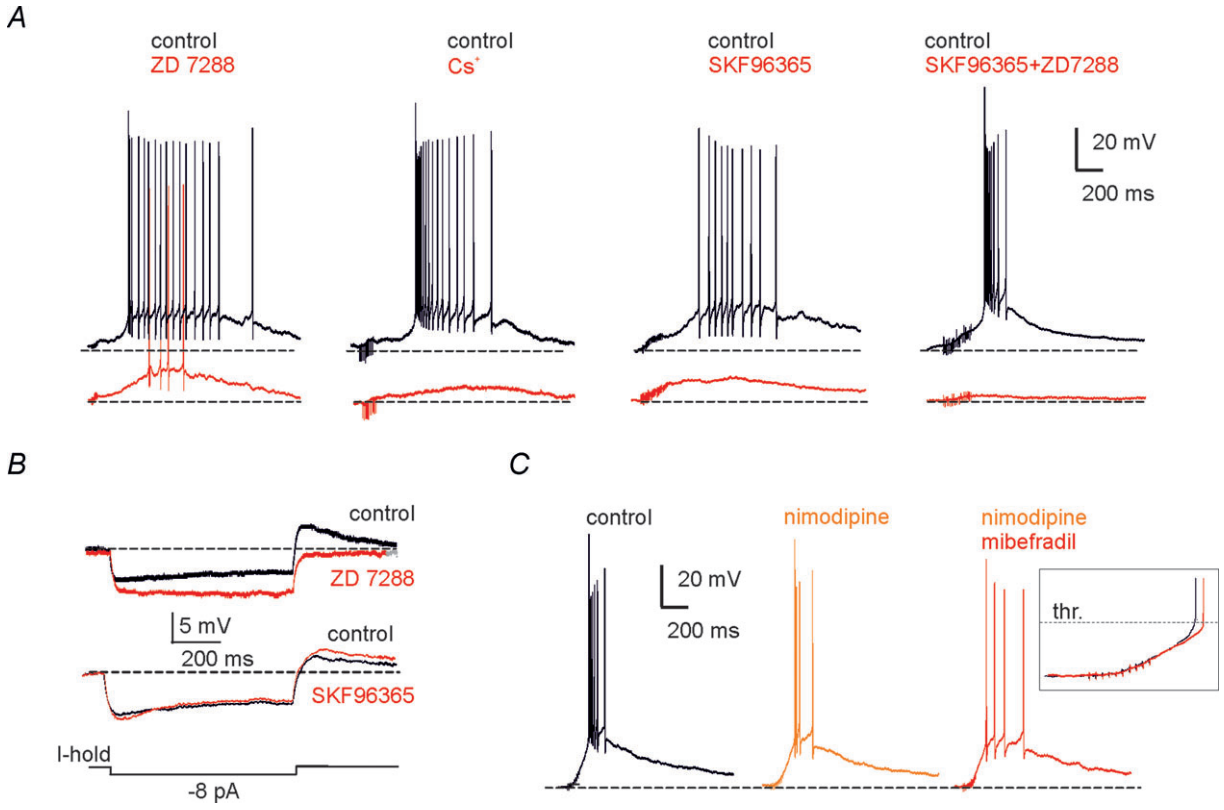

Figure 8. The late-onset burst is primed by H- and TRP-current activation
A, effects of different channel blockers on the late-onset response elicited by MFB stimulation, as follows: ZD7288 (2 μM), Cs^+ (2 mM), SKF96365 (30 μM), co-application of ZD7288 (2 μM) and SKF96365 (30 μM). In this and the following recordings the holding potential was maintained at −80 mV by adjusting the holding current. *B*, effect of ZD7288 (2 μM) and SKF96365 (30 μM) on the voltage response elicited by hyperpolarizing current step injection. *C*, effects of sequential application of nimodipine (20 μM) and mibefradil (10 μM) alone and in combination. The inset shows that the depolarizing ramp did not change significantly after nimodipine and mibefradil (20 min application), at least until the pre-potential just below spike threshold.

Table 1. Late-onset burst properties during pharmacological tests

	ZD7288 (2 μM)	ZD7288 (20 μM)	ZD7288 (2 and 20 μM)	Cs^+	SKF 96365	SKF 96365 + ZD7288 (2 μM)	Nimodipine	Nimodipine + Mibefradil
Depolarization (mV)	−29.66 ± 8.39% $n = 3$ $P < 0.1$ (2 μM) *vs.* (20 μM); $P = 0.44$	−37.64 ± 1.24% $n = 6$ $P < 0.0005$	−34.98 ± 2.88% $n = 9$ $P < 0.001$ ZD7288 *vs.* Cs^+; $P = 0.9$	−34.09 ± 6.67% $n = 4$ $P < 0.05$	−49.33 ± 6.06% $n = 5$ $P < 0.005$ SKF +ZD *vs.* SKF; $P < 0.01$ SKF +ZD *vs.* ZD; $P < 0.001$	−74.99 ± 4.44% $n = 5$ $P < 0.01$	4.19 ± 10.54% $n = 4$ $P = 0.7$ Nimodipine+Mibefradil *vs.* Nimodipine; $P = 0.7$	1.84 ± 3.52% $n = 3$ $P = 0.6$
Slope (mV ms^{-1})	−27.39 ± 6.43% $n = 5$ $P < 0.01$ (2 μM) *vs.* (20 μM); $P = 0.06$	−54.7 ± 9.92% $n = 6$ $P < 0.01$	−45.6 ± 8.08% $n = 9$ $P < 0.01$ ZD7288 *vs.* Cs^+; $P = 0.3$	−53.85 ± 9.39% $n = 4$ $P < 0.05$	−47.0 ± 5.13% $n = 5$ $P < 0.01$ SKF + ZD *vs.* SKF; $P < 0.01$ SKF +ZD *vs.* ZD; $P < 0.006$	−68.23 ± 9.77% $n = 5$ $P < 0.01$	−4.52 ± 5.72% $n = 4$ $P = 0.15$ Nimodipine+Mibefradil *vs.* Nimodipine; $P = 0.97$	−3.80 ± 17.9% $n = 3$ $P = 0.5$
Delay (ms)	65.32 ± 41.92% $n = 3$ $P < 0.05$ (2 μM) *vs.* (20 μM); $P = 0.5$	48.0 ± 11.18% $n = 6$ $P < 0.005$	52.93 ± 9.2% $n = 9$ $P < 0.001$	No spikes (4/4)	No spikes (4/5)	No spikes (5/5)	13.02 ± 8.77% $n = 4$ $P = 0.45$ Nimodipine+Mibefradil *vs.* Nimodipine; $P = 0.5$	3.22 ± 1.47% $n = 3$ $P = 0.66$
Duration (ms)	−47.41 ± 23.78% $n = 3$ $P < 0.05$ (2 μM) *vs.* (20 μM); $P = 0.4$	−34.32 ± 6.93% $n = 6$ $P < 0.05$	−39.24 ± 6.23% $n = 9$ $P < 0.05$	No spikes (4/4)	No spikes (4/5)	No spikes (5/5)	75.71 ± 32.16% $n = 4$ $P = 0.1$ Nimodipine+Mibefradil *vs.* Nimodipine; $P = 0.6$	39.44 ± 44.72% $n = 3$ $P = 0.5$

The table summarizes the measures of four parameters of the late-onset response (depolarization at the threshold time of the first spike in control, slope of the slow depolarizing ramp, delay to first spike in the burst, duration of the spike burst) during application of 2 or 20 μM ZD7288, 2 mM Cs^+, 30 μM SKF96365, 20 μM nimodipine and 10 μM mibefradil. The ensemble of ZD7288 measures is also reported, as there are no significant differences in any of the parameters between the two ZD7288 concentrations. The combined application of ZD7288 and SKF96365 leads to a significantly larger suppression of the late-onset response compared to each one of the antagonists applied alone. Nimodipine and mibefradil coapplication does not significantly improve the effect of mimodipine alone.

mossy fibre bundle stimulation. The distinctive properties of the two currents are that, while the H-current has a slow voltage-dependent activation, the TRP-current is almost instantaneous and voltage independent (Clapham, 2003). To reveal the stimulus-dependent changes in these currents, in UBCs showing the late-onset response the recording mode was switched to voltage clamp and membrane currents were measured before and after stimulation of the MFB (Fig. 10).

Both the current at the holding voltage of −70 mV and the current elicited by a hyperpolarizing voltage step to −130 mV increased following stimulation (Fig. 10*A*). The current change at the holding potential and the instantaneous current change during the step have to reflect both H- and TRP-channel activation (due to the increased driving force), while the time-dependent current change during the step can only be due to H-channel gating. On average, the holding current increased by 134.5 ± 25.9% ($n = 10$; $P < 0.002$, paired

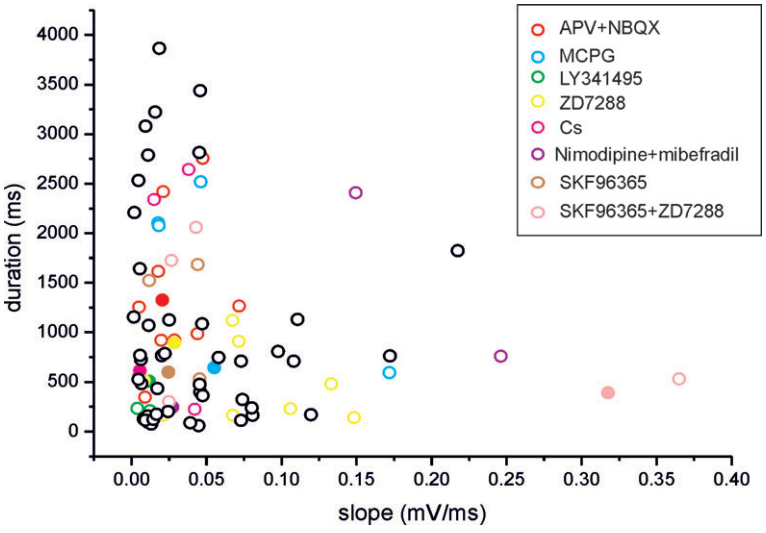

Figure 9. Features of the late-onset response
Scatter plot illustrating the correlation between the slope of the depolarizing ramp and the burst duration in the UBCs investigated ($n = 93$). Values refer to the late-onset response evoked by the minimal effective train (20 pulses) stimulation intensity to the MFB. Different colors refer to different experiments (see legend), with filled circles corresponding to experiments shown in the text.

t test), the instantaneous step-current increased by $44.1 \pm 10.0\%$ ($n = 10$; $P < 0.05$, paired *t* test) and the time-dependent step-current increased by $29.3 \pm 5.4\%$ ($n = 10$; $P < 0.001$, paired *t* test). Note that the current changes recovered with a time constant of a few seconds (3.6 ± 0.5 s; $n = 10$) (Fig. 10*A*), suggesting the intervention of a reversible modulatory process (see below).

The nature of currents involved in stimulus-dependent changes was assessed by blocking sequentially the TRP-channels with SKF96365 (30 μM) and H-channels with ZD7288 (2 μM), so that the TRP and H-currents could then be isolated by subtraction (Fig. 10*B*). At the end of the hyperpolarizing step, the TRP-current increased by $82.65 \pm 37.82\%$ ($n = 4$; $P < 0.05$) and the H-current increased by $33.17 \pm 5.23\%$ ($n = 4$; $P < 0.005$). Co-application of SKF96365 and ZD7288 almost completely suppressed the inward current changes, leaving a residual cumulative current increase of $10.77 \pm 1.62\%$ ($n = 4$, NS), suggesting that TRP and H-currents accounted almost entirely for the changes caused by MFB stimulation. Finally, in different experiments, intracellular perfusion of 500 μM cAMP through the patch pipette markedly prevented the effect

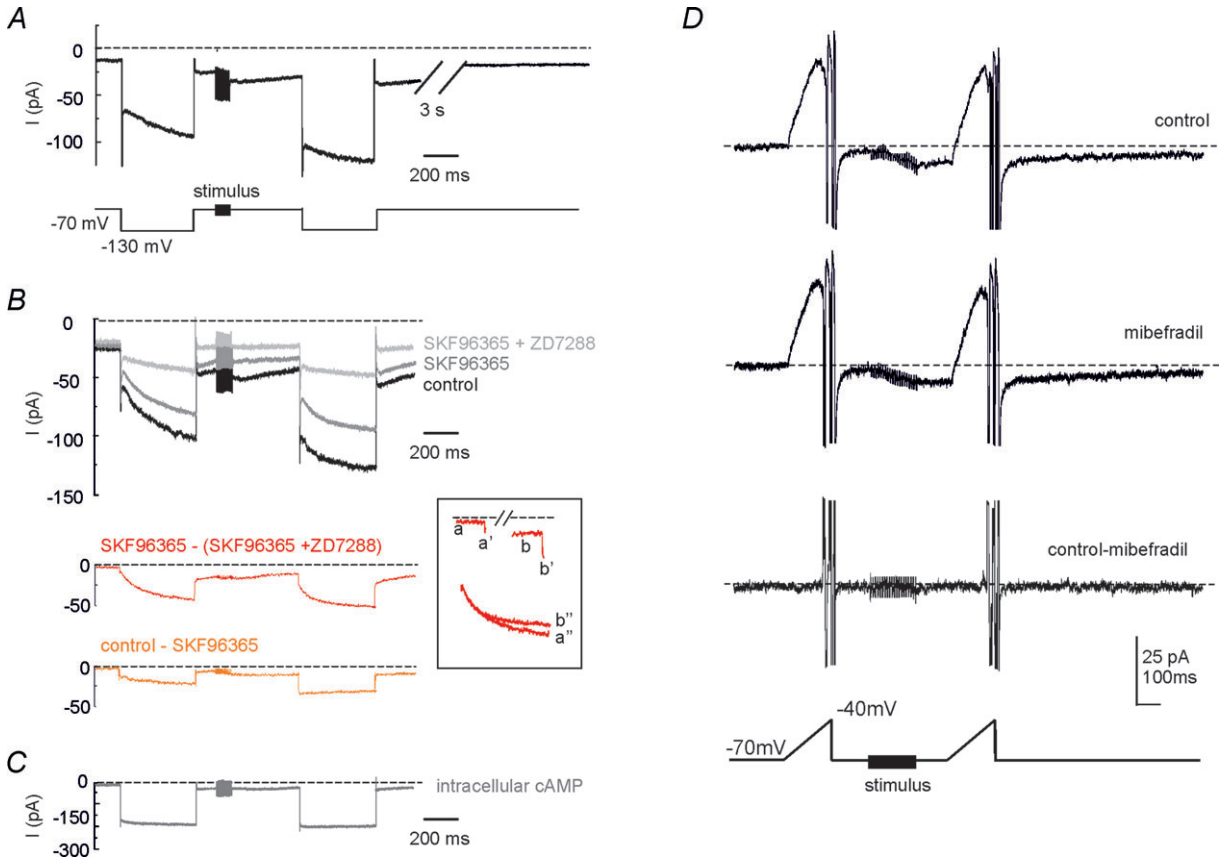

Figure 10. MFB stimulation increases H- and TRP-currents but not LVA current
A, voltage-clamp recording from a UBC showing the late-onset response when previously maintained in current clamp. Following MFB stimulation with a 20-pulse train, the inward current showed an increase both at the holding potential of −70 mV and during the voltage step at −130 mV. Upon return to −70 mV the current amplitude recovered to baseline in a few seconds. *B*, analogous experiment as in *A*, showing the effect of sequential application of ZD7288 (2 μM) and SKF96365 (30 μM). Bottom traces were obtained as difference currents and represent the H-current (SKF96365 – (SKF96365 + ZD7288)) and the TRP-current (control – SKF96365). The inset shows the relevant components of the H-current (a, b, holding current; a′, b′, instantaneous step current; a″, b″, time-dependent step current). *C*, analogous experiment as in *A* and *B*, but with a saturating concentration of cAMP (500 μM) in the patch-pipette solution. *D*, top: current response to a voltage-ramp from −70 to −40 mV (slope: 0.2 mV ms^{-1}), before and after MFB stimulation with a 20-pulse train. The ramp produced a large outward current in the subthreshold voltage range (action currents prevented subsequent activation of sodium channels). Note the shift in inward direction of the baseline following MFB stimulation. Middle: current response obtained after 20 min mibefradil application. Bottom: difference current. Note that the subthreshold current was unaffected by mibefradil either before or after train stimulation (see subtraction trace).

of MFB stimulation, leaving a residual current change of $6.12 \pm 2.26\%$ ($n = 4$) (Fig. 10*C*), indicating that H and TRP-channels are modulated through a cAMP-dependent pathway.

The potential depolarizing efficiency of these currents was evaluated by considering the H- and TRP-currents at the holding potential. Before the MFB stimulus, the TRP-current had an amplitude of -2.32 ± 1.04 pA and the H-current of -2.13 ± 1.26 pA ($n = 4$), suggesting a marginal resting activation. During the 300 ms after the train stimulus, the TRP-current increased up to -7.52 ± 0.91 pA and the H-current up to -12.44 ± 3.52 pA ($n = 4$), providing a substantial inward current capable of driving membrane depolarization up to the burst.

To further evaluate the current changes occurring after MFB stimulation, we measured the currents generated by depolarizing ramps (Fig. 10*D*) having similar slope and membrane potential range as measured in current-clamp recordings with mibefradil (cf. Fig. 8). During the ramp, a marked H-current deactivation was followed by action currents as the action potential threshold was reached. MFB stimulation caused an inward current (-8.15 ± 1.46 pA, $n = 4$, measured 50 ms after the end of the stimulus train; cf. Fig. 10*A*) followed by an increased outward current (9.28 ± 7.76 pA, $n = 4$, at the peak of H-current deactivation). The application of mibefradil did not affect the late-onset response currents so that the subtraction trace was flat (<1 pA difference compared to control), further ruling out that LVA calcium channels could take part to the depolarizing ramp leading to the late-onset burst.

Further evidence for the mechanisms of H-current modulation

In UBCs maintained in voltage clamp, the H-current was isolated by subtraction of the component blocked by ZD7288 (20 μM) from the total current (Fig. 11*A* and *B*). The H-current contributed to the holding current at -70 mV (-3.33 ± 5.12 pA, $n = 5$) and the *I–V* curve showed inward rectification (Fig. 11*C*). Boltzmann fittings to the *I–V* curve (Fig. 11*D*; cf. eqn 2) yielded a $G_{max} = 1.15$ nS, $V_{1/2} = -91.5$ mV, $k = 7.7$ mV^{-1} and $V_{rev} = -53$ mV. Note that these properties differed from those of the TRP-current, which was almost voltage-independent in the voltage range between -90 and -50 mV (see Fig. 11*C*, inset). The H-current activation time constant, measured using a mono-exponential fitting, decreased toward negative membrane potentials and showed average values ranging from ~180 ms at -130 mV to ~500 ms at -90 mV (Fig. 11*C*, inset; since the fitting was carried out over a limited time, slower current components could have gone undetected). Thus, the H-current was slowly depolarizing over the whole subthreshold range and between -50 and -70 mV it caused a ~3 mV depolarization (estimated by multiplying the current by input resistance), consistent with current-clamp measurements (cf. Fig. 8).

The way the H-current changed following MFB stimulation was complex, in that the increases in holding and instantaneous-step currents were apparently larger than the increase in time-dependent step current. A quantitative analysis of this effect on the recordings shown in Fig. 10 ($n = 4$) was performed by calling b/a the change in the holding current, b'/a' the change in the instantaneous step current, and b''/a'' the change in the time-dependent step current. If the H-current increased through a pure conductance modification, the current changes in the holding and in the step should be the same and the activation time constant should not be modified. However (Fig. 11*E*), the time-dependent step current decreased, while the holding and instantaneous step current increased. Accordingly, the change $b''/a'' = 0.77 \pm 0.21$ was significantly smaller than $b/a = 5.86 \pm 3.46$ ($n = 4$; $P < 0.005$) and $b'/a' = 1.91 \pm 0.32$ ($n = 4$; $P < 0.05$). Moreover, H-current activation became significantly faster (130.11 ± 5.41 ms *vs.* 187.23 ± 7.64 ms, $n = 4$; $P < 0.0005$, paired *t* test). The simplest explanation of this pattern is that synaptic activity modifies H-current gating, so that the steady-state and time-constant activation curves shift to the right, as in cardiac cells and neurons under cAMP control (Fig. 11*F*: see eqn 3) (DiFrancesco & Mangoni, 1994).

Discussion

Our main finding is that UBC synaptic activation is characterized by an early-onset and a late-onset response, both leading to action potential bursts. The early-onset response depended on the EPSPs generated by mossy fibre impulses, occurred with millisecond delay and was all-or-none in nature due to the high reliability of EPSP–spike coupling. Conversely, the late-onset response was independent of EPSPs, arose in tens to hundreds of milliseconds and was graded, in that its delay decreased (while its duration increased) with stimulus duration and intensity. The late-onset response was determined by activation of H- and TRP-currents, which increased following synaptic stimulation generating the depolarizing ramp priming the action potential burst. The action potential burst, but not the ramp, was influenced by calcium channels. The late-onset response represents a novel mechanism of neurotransmission and may play a role in encoding the afferent inputs to the vestibulo-cerebellum.

UBC electroresponsiveness: resting state and synaptic activation

The majority (>90%) of UBCs recorded in whole-cell configuration were quiescent with a resting membrane potential around −70 mV, similar to previous findings (Diana *et al.* 2007). That this could represent the native state of UBCs was supported by the absence of any spontaneous activity in LCA configuration, a condition in which the cytoplasmic integrity is preserved (Forti *et al.* 2006). The autorhythmic discharge in remaining (<10%) UBCs may reflect a specific regulation of background channels, including TRP (e.g. Russo *et al.* 2007), or

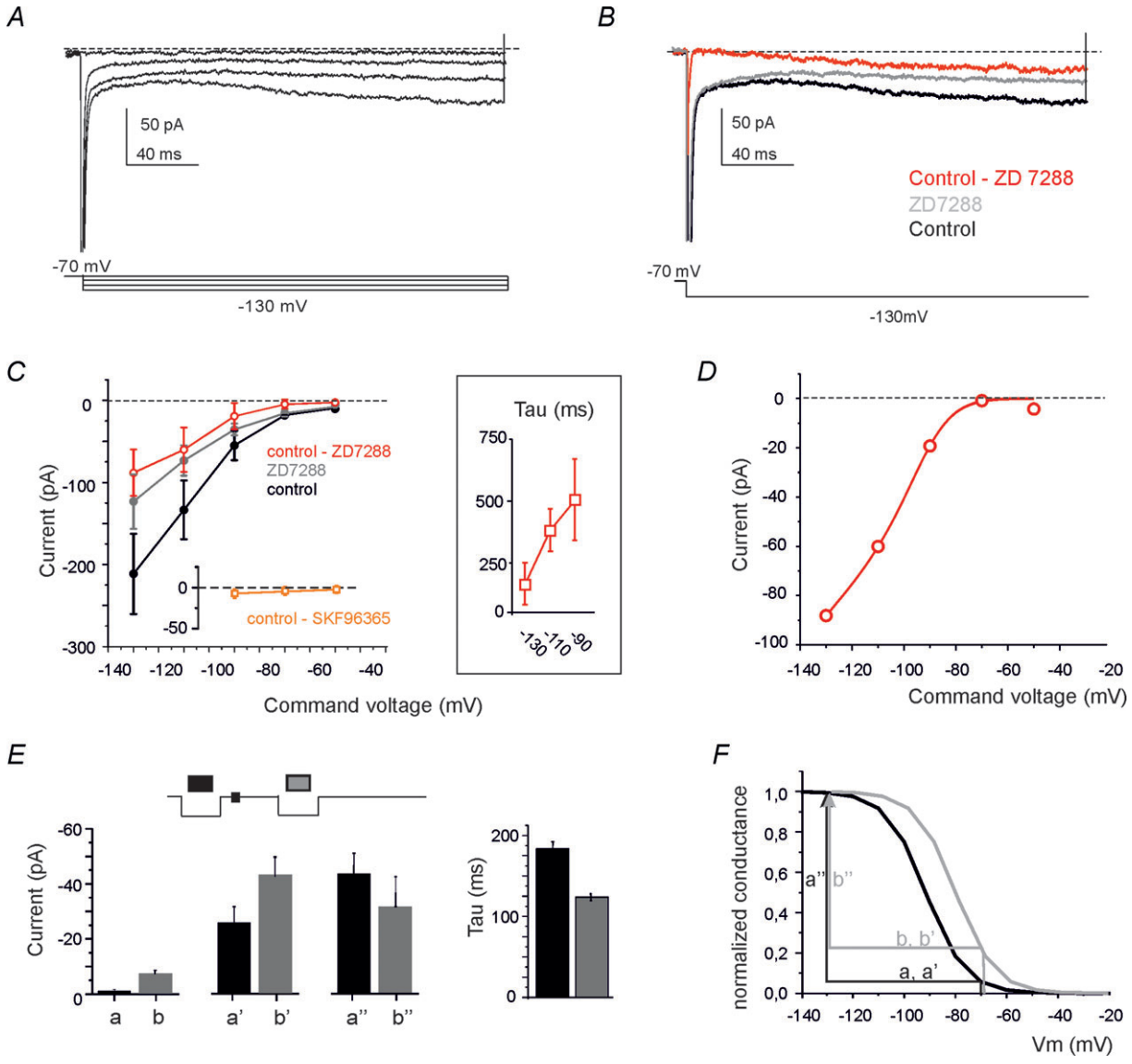

Figure 11. H-current modulation in UBCs
A, voltage-clamp recordings from a UBC showing H-current activation in response to hyperpolarizing voltage steps (the voltage protocol is shown at the bottom). *B*, the H-current (red trace) was isolated by subtraction of the current blocked by ZD7288 (20 μM) from the control current. *C*, *I–V* curves for current amplitude measured at the end of the hyperpolarizing pulses in control condition, after ZD7288 perfusion and for the ZD7288-sensitive current (H-current) ($n = 5$). The TRP-current (obtained as control – SKF96365) is reported for comparison on a separate axis. The inset shows the time constant of H-current activation. *D*, fitting of the H-current data points (taken from *C*) with a Boltzmann equation corrected for the driving force (eqn 2; see Methods). *E*, pattern of H-current changes (a, b, holding current; a′, b′, instantaneous current; a″, b″, time-dependent step current; cf. Fig. 7, inset following MFB stimulation). *F*, the pattern of changes reported in *A* can be explained by a rightward shift of the H-current conductance curve (reconstructed from eqn 3). The comparison of black and grey arrows shows that, after train stimulation, the proportion of channels open at −70 mV increases (b > a and b′ > a′) while the proportion of channels opened during the voltage step to −130 mV decreases (b″ < a″).

the expression of specific membrane receptors or calcium control mechanisms (Mugnaini *et al.* 2011).

By maintaining a low resting membrane potential and small background H- and TRP-channel activation, UBCs could fully exploit their ionic mechanisms to activate the depolarizing ramp in the late-onset response. At −70 mV, the H- and TRP-channels did not generate noticeable depolarizing current (∼−5 pA) but this was markedly increased by mossy fibre bundle stimulation (∼−20 pA). This current, given the input resistance of 0.8 GΩ, would produce a depolarization of ∼16 mV and therefore drive the cell above sodium action potential threshold (−56 mV). During UBC activity *in vivo*, the H- and TRP-channels could be differentially engaged. The continuous synaptic drive depolarizes UBCs generating protracted spike discharge (Ruigrok *et al.* 2011). This deactivates the H-current but the TRP-channels, which are poorly voltage dependent (see Fig. 11*C*, inset and Clapham, 2003), remain active. Synaptic inhibition generated by GABAergic and glycinergic fibres (Dugué *et al.* 2005; Rousseau *et al.* 2012) could hyperpolarize the cell, thus re-establishing the H-current and its action in the depolarizing ramp. Moreover, hyperpolarization could enhance the subsequent action potential burst by de-inactivating LVA calcium channels.

Ionic mechanisms of the late-onset response

Despite the apparent similarity of their spike bursts, the mechanisms of the early-onset and late-onset responses differed remarkably. The early-onset response was generated by AMPA and NMDA receptor-mediated EPSPs amplified by glutamate spillover (Rossi *et al.* 1995). Conversely, the late-onset response did not require either ionotropic or mGluRs, at least those of class I and II sensitive to MCPG and LY341495, which are expressed in UBCs (Russo *et al.* 2008; Rousseau *et al.* 2012). In fact, the depolarizing ramp of the late-onset response was sustained by H- and TRP-channels. In both the early- and the late-onset response, the subthreshold depolarization was coupled with a spike burst sustained by LVA and HVA Ca^{2+} channels (Diana *et al.* 2007).

The occluding effect of intracellular cAMP on the H- and TRP currents raised by mossy fibre bundle stimulation suggests that the corresponding channels are modulated by this cyclic nucleotide. The time required to raise cAMP and to gate ionic channels can range up to hundreds of milliseconds, providing an explanation for the long delays shown by the late-onset response. Both H- and TRP-channels are usually modulated by cAMP (Wainger *et al.* 2001; Clapham, 2003). In particular, the pattern of changes observed in the H-current following mossy fibre bundle stimulation suggests a reversible modification of the gating mechanism, in which the H-current activation curve and the time constant curve shift to the right (see Fig. 11*F*). These results are consistent with an increased opening probability of H-channels, as reported in the sino-atrial node cells of the heart (DiFrancesco & Mangoni, 1994) and in neurons (Wainger *et al.* 2001; Santoro *et al.* 2009, 2011).

The H-current in neurons is usually generated by a blend of channel subtypes (HCN1–4) (Santoro *et al.* 2000). The combination of the different subtypes determines different sensitivity to cAMP, which can in turn modify their gating and kinetics (Wainger *et al.* 2001; Santoro *et al.* 2009, 2011). Immunolabelling shows that UBCs express both HCN1 and HCN2 subtypes (Santoro *et al.* 2009). In reconstituted systems, HCN1 shows faster kinetics than HCN2, but the latter has higher cAMP sensitivity (Wainger *et al.* 2001). The combination of HCN1 and HCN2 in heteromeric channels is relatively fast (like HCN1) and cAMP sensitive (like HCN2). According to our estimates, the H-current first activation time constant is in the 100 ms range and the cAMP shift is in the 10 mV range. Therefore, the H-current of UBCs shows properties consistent with that of HCN1–HCN2 heteromers, in line with the colocalization of HCN1 and HCN2 channel subunits.

Synaptic mechanisms of the late-onset response

A puzzling observation is that the delay of the late-onset response decreased with the intensity and number of MFB stimuli, while it is well known that a single mossy fibre impinges on the UBC brush (Rossi *et al.* 1995). This was consistently demonstrated by the all-or-none early-onset responses shown in Fig. 2*A*–*C*. Therefore, the regulation of delay could reflect the recruitment of fibres other than the one impinging on the UBC brush and acting through extrasynaptic diffusion of a (yet unknown) neurotransmitter. The amount of such transmitter could then modulate the cAMP level and H- and TRP-currents in the UBC in a dose-dependent manner. The neuropeptidergic system related to dense-core vesicles, which are present in mossy fibre terminals and may be co-released with glutamate (Mugnaini *et al.* 1997), is especially attractive due to its graded recruitment with stimulus trains and to its ability to generate delayed responses in neurons (Park & Kim, 2009). Immunolabelling analysis may be used to anticipate the nature of putative neuromodulatory peptides. Other potential candidates are cholinergic (Jaarsma *et al.* 1996, 1997), noradrenergic (Yamada *et al.* 2005) or serotoninergic (Bickmeyer *et al.* 2002) fibres, which coexist with glutamatergic mossy fibres in the cerebellum and may be activated by stimulating the MFB. Also these systems exert a paracrine action on their targets and are potentially capable of generating delayed protracted neuronal responses through ionic channel modulation

(Brown *et al.* 1981; Siegelbaum *et al.* 1982; see also below). The aminergic systems may be independently activated by stimulating their brainstem nuclei *in vivo*.

Comparison with other slow synaptic responses in neurons

Although there are several reports on protracted synaptic depolarization and slow EPSPs, the corresponding mechanisms appear to be the most diverse. Originally, serotonin was shown to modulate potassium currents with an increase in post-synaptic responses in aplysia neurons (Siegelbaum *et al.* 1982) and muscarinic receptors were shown to generate a slow EPSP by inhibiting the M current in bullfrog sympathetic ganglion neurons (Brown *et al.* 1981). More recently, NMDA receptors were reported to activate TRP-channels generating a protracted depolarization in granule cells of the olfactory bulb (Stroh *et al.* 2012), while mGluRs (mGluR1) were shown to activate TRP-channels generating slow EPSPs in Purkinje cells of the cerebellum (Batchelor *et al.* 1994; Tempia *et al.* 2001; Kim *et al.* 2003; Hartmann & Konnerth, 2008). A candidate homologous of the late-onset response of UBCs could be the delayed protracted synaptic response observed in globus pallidus neurons, which is generated monosynaptically through as yet unknown ionic mechanisms and is (at least partially) independent of glutamate receptor activation (Kaneda *et al.* 2007). Therefore, although the presence of delayed protracted synaptic depolarizations appears recurrently in nature, the late-onset response observed in UBCs, which involves a glutamate receptor-independent cAMP-dependent up-regulation of TRP- and H-currents, seems to be unique in its kind.

Conclusions and functional implications

The late-onset response allows UBCs to generate graded outputs, which would otherwise be impossible due to the all-or-none behaviour of the early-onset response. Through the late-onset response, UBCs can translate the intensity of the input (coded as the number of active fibres and duration of their discharge) into output bursts with different delay. This implements a time-code that could reverberate through the network along the chains made by UBCs with other UBCs and granule cells (Nunzi & Mugnaini, 2000; Nunzi *et al.* 2001). The late-onset response mechanisms could be modulated depending on local network control on the state of UBC activation and inhibition (Ruigrok *et al.* 2011; Rousseau *et al.* 2012). The late-onset responses originating in the UBC circuits, by generating a distribution of granular layer delays over a long time scale (hundreds of milliseconds), overlaps with the shorter response delays controlled through the time-window mechanism implemented by the mossy fibre–granule cell–Golgi cell circuit (D'Angelo & De Zeeuw, 2009). Thus, the late-onset response could extend the timing capabilities of the granular layer.

The late-onset UBC response might help in implementing the 'velocity storage' system (Dai *et al.* 2007), which allows the vestibulo-cerebellum to transform the head velocity signal into commands for ocular motor neurons controlling the slow phase of nystagmus (Goldberg *et al.* 1984; Okada *et al.* 1999). A slow head rotation producing a weak vestibular input would generate a late-onset burst with significant delay, while a fast head rotation producing a stronger input would generate a late-onset burst with shorter delay. In this respect, the late-onset response is more suitable than the early-onset response (Diño *et al.* 2000; Simpson *et al.* 2005), since the latter has fixed short delay. As much as the late-onset response could be important to store kinematic parameters related to head movement in the vestibulo-cerebellum, it could likewise help to store different kinds of neural information for hundreds of milliseconds to seconds in other parts of the cerebellum and in the cochlear nucleus (Mugnaini *et al.* 1997), where UBCs have also been observed.

References

Batchelor AM, Madge DJ & Garthwaite J (1994). Synaptic activation of metabotropic glutamate receptors in the parallel fibre–Purkinje cell pathway in rat cerebellar slices. *Neuroscience* **63**, 911–915.

Bickmeyer U, Heine M, Manzke T & Richter DW (2002). Differential modulation of I_h by 5-HT receptors in mouse CA1 hippocampal neurons. *Eur J Neurosci* **16**, 209–218.

Brown DA, Constanti A & Adams PR (1981). Slow cholinergic and peptidergic transmission in sympathetic ganglia. *Fed Proc* **40**, 2625–2630.

Clapham DE (2003). TRP channels as cellular sensors. *Nature* **426**, 517–524.

D'Angelo E, De Filippi G, Rossi P & Taglietti V (1995). Synaptic excitation of individual rat cerebellar granule cells *in situ*: evidence for the role of NMDA receptors. *J Physiol* **484**, 397–413.

D'Angelo E, De Filippi G, Rossi P & Taglietti V (1997). Synaptic activation of Ca^{2+} action potentials in immature rat cerebellar granule cells in situ. *J Neurophysiol* **78**, 1631–1642.

D'Angelo E, De Filippi G, Rossi P & Taglietti V (1998). Ionic mechanism of electroresponsiveness in cerebellar granule cells implicates the action of a persistent sodium current. *J Neurophysiol* **80**, 493–503.

D'Angelo E & De Zeeuw CI (2009). Timing and plasticity in the cerebellum: focus on the granular layer. *Trends Neurosci* **32**, 30–40.

D'Angelo E, Rossi P & Taglietti V (1993). Different proportions of *N*-methyl-D-aspartate and non-*N*-methyl-D-aspartate receptor currents at the mossy fibre-granule cell synapse of developing rat cerebellum. *Neuroscience* **53**, 121–130.

Dai M, Raphan T & Cohen B (2007). Labyrinthine lesions and motion sickness susceptibility. *Exp Brain Res* **178**, 477–487.

Diana MA, Otsu Y, Maton G, Collin T, Chat M & Dieudonné S (2007). T-type and L-type Ca^{2+} conductances define and encode the bimodal firing pattern of vestibulocerebellar unipolar brush cells. *J Neurosci* **27**, 3823–3838.

Dickson CT, Magistretti J, Shalinsky MH, Fransén E, Hasselmo ME & Alonso A (2000). Properties and role of I_h in the pacing of subthreshold oscillations in entorhinal cortex layer II neurons. *J Neurophysiol* **83**, 2562–2579.

Dieudonne S (1998). Submillisecond kinetics and low efficacy of parallel fibre–Golgi cell synaptic currents in the rat cerebellum. *J Physiol* **510**, 845–866.

DiFrancesco D & Mangoni M (1994). Modulation of single hyperpolarization-activated channels (i_f) by cAMP in the rabbit sino-atrial node. *J Physiol* **474**, 473–482.

Diño MR, Nunzi MG, Anelli R & Mugnaini E (2000). Unipolar brush cells of the vestibulocerebellum: afferents and targets. *Prog Brain Res* **124**, 123–137.

Diño MR, Perachio AA & Mugnaini E (2001). Cerebellar unipolar brush cells are targets of primary vestibular afferents: an experimental study in the gerbil. *Exp Brain Res* **140**, 162–170.

Do MT & Bean BP (2003). Subthreshold sodium currents and pacemaking of subthalamic neurons: modulation by slow inactivation. *Neuron* **39**, 109–120.

Dugué GP, Dumoulin A, Triller A & Dieudonné S (2005). Target-dependent use of co-released inhibitory transmitters at central synapses. *J Neurosci* **25**, 6490–6498.

Forti L, Cesana E, Mapelli J & D'Angelo E (2006). Ionic mechanisms of autorhythmic firing in rat cerebellar Golgi cells. *J Physiol* **574**, 711–729.

Funahashi M, Mitoh Y, Kohjitani A & Matsuo R (2003). Role of the hyperpolarization-activated cation current (I_h) in pacemaker activity in area postrema neurons of rat brain slices. *J Physiol* **552**, 135–148.

Gall D, Roussel C, Susa I, D'Angelo E, Rossi P, Bearzatto B, Galas MC, Blum D & Schiffmann SN (2003). Altered neuronal excitability in cerebellar granule cells of mice lacking calretinin. *J Neurosci* **23**, 9320–9327.

Gasparini S & DiFrancesco D (1997). Action of the hyperpolarization-activated current (I_h) blocker ZD 7288 in hippocampal CA1 neurons. *Pflugers Arch* **435**, 99–106.

Goldberg JM, Smith CE & Fernández C (1984). Relation between discharge regularity and responses to externally applied galvanic currents in vestibular nerve afferents of the squirrel monkey. *J Neurophysiol* **51**, 1236–1256.

Hartmann J & Konnerth A (2008). Mechanisms of metabotropic glutamate receptor-mediated synaptic signaling in cerebellar Purkinje cells. *Acta Physiol* **195**, 79–90.

Hille B & Schwarz W (1978). Potassium channels as multi-ion single-file pores. *J Gen Physiol* **72**, 409–442.

Jaarsma D, Diño MR, Cozzari C & Mugnaini E (1996). Cerebellar choline acetyltransferase positive mossy fibres and their granule and unipolar brush cell targets: a model for central cholinergic nicotinic neurotransmission. *J Neurocytol* **25**, 829–842.

Jaarsma D, Ruigrok TJ, Caffé R, Cozzari C, Levey AI, Mugnaini E & Voogd J (1997). Cholinergic innervation and receptors in the cerebellum. *Prog Brain Res* **114**, 67–96.

Kalinichenko SG & Okhotin VE (2005). Unipolar brush cells–a new type of excitatory interneuron in the cerebellar cortex and cochlear nuclei of the brainstem. *Neurosci Behav Physiol* **35**, 21–36.

Kaneda K, Kita T & Kita H (2007). Repetitive activation of glutamatergic inputs evokes a long-lasting excitation in rat globus pallidus neurons *in vitro*. *J Neurophysiol* **97**, 121–133.

Kim SJ, Kim YS, Yuan JP, Petralia RS, Worley PF & Linden DJ (2003). Activation of the TRPC1 cation channel by metabotropic glutamate receptor mGluR1. *Nature* **426**, 285–291.

Kinney GA, Overstreet LS & Slater NT (1997). Prolonged physiological entrapment of glutamate in the synaptic cleft of cerebellar unipolar brush cells. *J Neurophysiol* **78**, 1320–1333.

Maccaferri G & McBain CJ (1996). The hyperpolarization-activated current (I_h) and its contribution to pacemaker activity in rat CA1 hippocampal stratum oriens-alveus interneurones. *J Physiol* **497**, 119–130.

Maffei A, Prestori F, Rossi P, Taglietti V & D'Angelo E (2002). Presynaptic current changes at the mossy fiber–granule cell synapse of cerebellum during LTP. *J Neurophysiol* **88**, 627–638.

Mapelli L, Rossi P, Nieus T & D'Angelo E (2009). Tonic activation of $GABA_B$ receptors reduces release probability at inhibitory connections in the cerebellar glomerulus. *J Neurophysiol* **101**, 3089–3099.

Mugnaini E, Diño MR & Jaarsma D (1997). The unipolar brush cells of the mammalian cerebellum and cochlear nucleus: cytology and microcircuitry. *Prog Brain Res* **114**, 131–150.

Mugnaini E, Sekerkova G & Martina M (2011). The unipolar brush cell: a remarkable neuron finally receiving deserved attention. *Brain Res Rev* **66**, 220–245.

Neuhoff H, Neu A, Liss B & Roeper J (2002). I_h Channels contribute to the different functional properties of identified dopaminergic subpopulations in the midbrain. *J Neurosci* **22**, 1290–1302.

Nolan MF, Malleret G, Dudman JT, Buhl DL, Santoro B, Gibbs E, Vronskaya S, Buzsaki G, Siegelbaum SA, Kandel ER & Morozov A (2004). A behavioral role for dendritic integration: HCN1 channels constrain spatial memory and plasticity at inputs to distal dendrites of CA1 pyramidal neurons. *Cell* **119**, 719–732.

Nolan MF, Malleret G, Lee KH, Gibbs E, Dudman JT, Santoro B, Yin D, Thompson RF, Siegelbaum SA, Kandel ER & Morozov A (2003). The hyperpolarization-activated HCN1 channel is important for motor learning and neuronal integration by cerebellar Purkinje cells. *Cell* **115**, 551–564.

Nunzi MG, Birnstiel S, Bhattacharyya BJ, Slater NT & Mugnaini E (2001). Unipolar brush cells form a glutamatergic projection system within the mouse cerebellar cortex. *J Comp Neurol* **434**, 329–341.

Nunzi MG & Mugnaini E (2000). Unipolar brush cell axons form a large system of intrinsic mossy fibers in the postnatal vestibulocerebellum. *J Comp Neurol* **422**, 55–65.
Okada T, Grunfeld E, Shallo-Hoffmann J & Bronstein AM (1999). Vestibular perception of angular velocity in normal subjects and in patients with congenital nystagmus. *Brain* **122**, 1293–1303.
Park Y & Kim KT (2009). Short-term plasticity of small synaptic vesicle (SSV) and large dense-core vesicle (LDCV) exocytosis. *Cell Signal* **21**, 1465–1470.
Prestori F, Rossi P, Bearzatto B, Laine J, Necchi D, Diwakar S, Schiffmann SN, Axelrad H & D'Angelo E (2008). Altered neuron excitability and synaptic plasticity in the cerebellar granular layer of juvenile prion protein knock-out mice with impaired motor control. *J Neurosci* **28**, 7091–7103.
Rossi DJ, Alford S, Mugnaini E & Slater NT (1995). Properties of transmission at a giant glutamatergic synapse in cerebellum: the mossy fiber–unipolar brush cell synapse. *J Neurophysiol* **74**, 24–42.
Rossi P, Mapelli L, Roggeri L, Gall D, de Kerchove d'Exaerde A, Schiffmann SN, Taglietti V & D'Angelo E (2006). Inhibition of constitutive inward rectifier currents in cerebellar granule cells by pharmacological and synaptic activation of GABA receptors. *Eur J Neurosci* **24**, 419–432.
Rousseau CV, Dugue GP, Dumoulin A, Mugnaini E, Dieudonne S & Diana MA (2012). Mixed inhibitory synaptic balance correlates with glutamatergic synaptic phenotype in cerebellar unipolar brush cells. *J Neurosci* **32**, 4632–4644.
Ruigrok TJ, Hensbroek RA & Simpson JI (2011). Spontaneous activity signatures of morphologically identified interneurons in the vestibulocerebellum. *J Neurosci* **31**, 712–724.
Russo MJ, Mugnaini E & Martina M (2007). Intrinsic properties and mechanisms of spontaneous firing in mouse cerebellar unipolar brush cells. *J Physiol* **581**, 709–724.
Russo MJ, Yau HJ, Nunzi MG, Mugnaini E & Martina M (2008). Dynamic metabotropic control of intrinsic firing in cerebellar unipolar brush cells. *J Neurophysiol* **100**, 3351–3360.
Sanchez-Alonso JL, Halliwell JV & Colino A (2008). ZD 7288 inhibits T-type calcium current in rat hippocampal pyramidal cells. *Neurosci Lett* **439**, 275–280.
Santoro B, Chen S, Luthi A, Pavlidis P, Shumyatsky GP, Tibbs GR & Siegelbaum SA (2000). Molecular and functional heterogeneity of hyperpolarization-activated pacemaker channels in the mouse CNS. *J Neurosci* **20**, 5264–5275.
Santoro B, Hu L, Liu H, Saponaro A, Pian P, Piskorowski RA, Moroni A & Siegelbaum SA (2011). TRIP8b regulates HCN1 channel trafficking and gating through two distinct C-terminal interaction sites. *J Neurosci* **31**, 4074–4086.
Santoro B, Piskorowski RA, Pian P, Hu L, Liu H & Siegelbaum SA (2009). TRIP8b splice variants form a family of auxiliary subunits that regulate gating and trafficking of HCN channels in the brain. *Neuron* **62**, 802–813.
Shepherd G (2003). *The Synaptic Organization of the Brain.* Oxford University Press, Oxford.
Siegelbaum SA, Camardo JS & Kandel ER (1982). Serotonin and cyclic AMP close single K^+ channels in aplysia sensory neurones. *Nature* **299**, 413–417.
Silver RA, Cull-Candy SG & Takahashi T (1996). Non-NMDA glutamate receptor occupancy and open probability at a rat cerebellar synapse with single and multiple release sites. *J Physiol* **494**, 231–250.
Simpson JI, Hulscher HC, Sabel-Goedknegt E & Ruigrok TJ (2005). Between in and out: linking morphology and physiology of cerebellar cortical interneurons. *Prog Brain Res* **148**, 329–340.
Singh A, Hildebrand ME, Garcia E & Snutch TP (2010). The transient receptor potential channel antagonist SKF96365 is a potent blocker of low-voltage-activated T-type calcium channels. *Br J Pharmacol* **160**, 1464–1475.
Sola E, Prestori F, Rossi P, Taglietti V & D'Angelo E (2004). Increased neurotransmitter release during long-term potentiation at mossy fibre–granule cell synapses in rat cerebellum. *J Physiol* **557**, 843–861.
Solinas S, Forti L, Cesana E, Mapelli J, De Schutter E & D'Angelo E (2007a). Computational reconstruction of pacemaking and intrinsic electroresponsiveness in cerebellar Golgi cells. *Front Cell Neurosci* **1**, 2.
Solinas S, Forti L, Cesana E, Mapelli J, De Schutter E & D'Angelo E (2007b). Fast-reset of pacemaking and theta-frequency resonance patterns in cerebellar golgi cells: simulations of their impact *in vivo*. *Front Cell Neurosci* **1**, 4.
Stroh O, Freichel M, Kretz O, Birnbaumer L, Hartmann J & Egger V (2012). NMDA receptor-dependent synaptic activation of TRPC channels in olfactory bulb granule cells. *J Neurosci* **32**, 5737–5746.
Tempia F, Alojado ME, Strata P & Knöpfel T (2001). Characterization of the $mGluR_1$-mediated electrical and calcium signaling in Purkinje cells of mouse cerebellar slices. *J Neurophysiol* **86**, 1389–1397.
Wainger BJ, DeGennaro M, Santoro B, Siegelbaum SA & Tibbs GR (2001). Molecular mechanism of cAMP modulation of HCN pacemaker channels. *Nature* **411**, 805–810.
Yamada R, Kuba H, Ishii TM & Ohmori H (2005). Hyperpolarization-activated cyclic nucleotide-gated cation channels regulate auditory coincidence detection in nucleus laminaris of the chick. *J Neurosci* **25**, 8867–8877.

Author contributions

F.L. performed most of the experiments and analysis and was initially aided by L.B. F.P. supervised the experiments and analysis. S.M. and E.D. coordinated the work and E.D. wrote the final version of the manuscript. All authors approved the final version.

Acknowledgements

This work was supported by the European Union (CEREBNET FP7-ITN238686, REALNET FP7-ICT270434) to E.D. and by a grant of the Ministero della Ricerca to S.M. We thank G. Ferrari and M. Rossin for technical support.